

2 **Detection of dietary stress and geophagic behaviour forced by dry seasons in Miocene**
3 ***Gomphotherium***

4 Rute Coimbra ^(a), Niels de Winter ^(b,c), Maria Ríos ^(d,e), Rui Bernardino ^(f), Darío Estraviz-López ^(d,e), Priscila
5 Lohmann ^(d), Roberta Martino ^(d,e), Aurora Grandal-d'Anglade ^(g), Fernando Rocha ^(a), Philippe Claeys ^(c)

6
7 (a) Geobiotec, Dpt. of Geosciences, University of Aveiro, Portugal

8 (b) Dept. of Earth Sciences, Vrije Universiteit Amsterdam, Netherlands

9 (c) Archaeology, Environmental Changes & Geo-chemistry group, Vrije Universiteit Brussel, Belgium

10 (d) Dpt. of Earth Sciences, NOVA School of Science and Technology, Universidade Nova de Lisboa,
11 GeoBioTec, Caparica, Portugal

12 (e) Museu da Lourinhã, Lourinhã, Portugal

13 (f) Jardim Zoológico de Lisboa, Lisboa, Portugal

14 (g) ESCI, Instituto Universitario de Xeoloxía, Universidade da Coruña, A Coruña, Spain

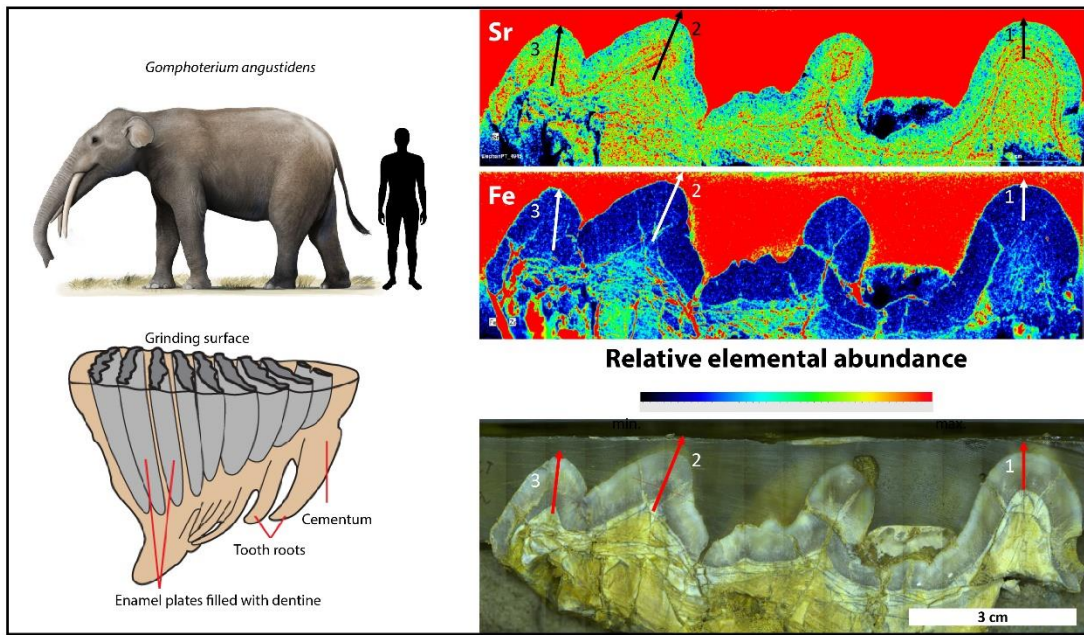
15
16
17 **Corresponding author and first author:**

18 Rute Coimbra rcoimbra@ua.pt

19
20
21 **Abstract**

22 To access the impact of anthropogenic emissions and land use change on Earth's climate and
23 biodiversity, studies into the environment and ecology of natural ecosystems during past warm periods
24 are required. The Miocene Climatic Optimum is a key reference period for future global warming
25 scenarios. However, studies uncovering Miocene climate have heavily favoured marine environments,
26 leaving the impact of warming on terrestrial ecosystems understudied. Here, we present a multi-
27 disciplinary study into the chemical composition of fossil *Gomphotherium angustidens* (Proboscidea,
28 Mammalia) teeth from the Middle Miocene Vb division (~15.9–16.1Ma) of western Portugal (Chelas
29 Valley, Lisbon, Lusitanian basin) and their sedimentological context. Trace element and stable isotope
30 compositions in these fossil teeth are compared with similar measurements in molars of a
31 taxonomically related modern African elephant (captive *Loxodonta africana*). Results reveal seasonal-
32 scale variability in trace elements in both fossil and modern proboscidean tooth enamel, which are
33 interpreted as evidence for seasonal changes in diet. Periodic increases in Na, Fe and Si in *G.*
34 *angustidens* demonstrate intake of sediment in the diet during fixed times of the year, a behaviour type
35 previously described in modern elephants during dry seasons. In combination with the heavier carbon
36 and oxygen isotopic composition in *G. angustidens* compared to *L. africana*, the terrestrial climate in
37 Miocene Portugal appears characterized by seasonally dry periods, which forced geophagy behaviour
38 of these large mammals and likely had significant consequences for the composition of Miocene
39 ecosystems (e.g., food/water availability and potential seasonal range shifts) in southwestern Europe.

44 Graphical abstract



45

46 1. Introduction

47 1.1 The Middle Miocene as a reference period for warm climate

48 The study of historical variations in climate and environment has emerged as a potent method for
49 understanding the scale, duration, and trajectory of global change. This approach also aids in assessing
50 and forecasting potential outcomes in future scenarios, as underscored by the Intergovernmental Panel
51 on Climate Change (IPCC) in its 6th assessment report (IPCC, 2023). The Middle Miocene Climate
52 Optimum (MCO; 17 – 15 Ma) represents a period of major global warming within the Cenozoic cooling
53 trend (Domingo et al., 2009; Harzhauser et al., 2011; Meckler et al., 2022; Westerhold et al., 2020).
54 This brief hot period, reaching ~ 600 ppm atmospheric CO₂, closely mimics projections for future
55 temperatures under a moderate IPCC warming (Meinshausen et al., 2020; Methner et al., 2020; Super
56 et al., 2018). Therefore, MCO constitutes an appropriate analogue to access the predictive nature of
57 climate models (Burls et al., 2021; Goldner et al., 2014; Holbourn et al., 2015; Steinthorsdottir et al.,
58 2020).

59

60 Employing biogeochemical techniques to extract short-term geochemical information from fossil
61 skeletal remains constitutes a highly informative method, as it enables the characterization of past
62 global changes for a timespan that far exceeds instrumental records (Meckler et al., 2022; Westerhold
63 et al., 2020; Zachos et al., 2001, 2008). A deeper exploration of the marine geological record has been
64 carried out from a biogeochemical perspective, specifically utilizing stable oxygen isotope ratios ($\delta^{18}\text{O}$)
65 as proxies for past ocean water density (salinity and/or temperature). The $\delta^{18}\text{O}$ proxy has been
66 primarily used in the study of marine paleoarchives (Westerhold et al., 2020; Zachos et al., 2008). Since
67 a similarly detailed approach is missing from the continental realm, it is crucial to enhance
68 biogeochemical investigations into proxies reflecting terrestrial records to achieve a comprehensive
69 understanding of the climatic, environmental, and ecological changes that have shaped the planet.

70 Gomphotheres filled a similar niche as modern African elephants, likely shaping their environments
71 much like modern elephants do, so their history gives us a window into what happens when a major
72 ecosystem-engineer faces rapid change (Cantalapiedra et al., 2021). If elephants today struggle with
73 warming, drought, or shifting vegetation, their ecosystems will be impacted. They disperse seeds, open
74 habitats, keep woody cover in check, and move nutrients, processes that strongly affect biodiversity
75 and even carbon cycling (Malhi et al., 2016). When past megaherbivores declined, those functions
76 vanished, and landscapes became less resilient (Gill et al., 2009). Understanding the ecology and
77 vulnerability of megaherbivores is therefore of crucial importance for assessing the stability of
78 ecosystems and their resilience to climate and environmental change.

79

80 1.2 Bioapatite as an environmental archive

81 Bioapatite ($\text{Ca}_{10}(\text{PO}_4, \text{CO}_3)_6(\text{OH}, \text{F})$; (LeGeros, 1986)), the material from which teeth and bones in
82 terrestrial vertebrates are made, constitutes a promising archive for recording short-term
83 environmental variability in the terrestrial realm. Bioapatite is one of the strongest biogenic materials
84 and has excellent fossilization potential (Lee-Thorp and Sponheimer, 2003). The oxygen isotope
85 composition of carbonate ($\delta^{18}\text{O}_c$) structurally bound to bioapatite in skeletal tissues primarily reflects
86 the climatic and environmental conditions experienced by the examined individual during its life
87 (Cerling et al., 1997a; de Winter and Claeys, 2016; Fricke and O'Neil, 1996). For terrestrial vertebrates,
88 these measurements mirror the $\delta^{18}\text{O}$ content of body water, which, in turn, captures the $\delta^{18}\text{O}$
89 composition of meteoric water after correcting for metabolic fractionation, and are related to the
90 mineralization temperature of the mineral (Ayliffe et al., 1992). Furthermore, with increasing aridity,
91 the enrichment of ^{18}O in meteoric and vegetation water, and therefore in tooth enamel, intensifies due
92 to evaporation effects- Rayleigh fractionation (Tütken et al., 2007). Hence, the bioapatite $\delta^{18}\text{O}_c$

93 signature found in fossil vertebrates serves as a valuable source of information about temperature and
94 aridity levels within terrestrial environments (Koch et al., 2007).

95 Initial investigations into the carbon isotope value of bioapatite ($\delta^{13}\text{C}_{\text{ap}}$) in terrestrial vertebrates
96 revealed its capacity to document dietary choices, facilitating the reconstruction of habitats (such as
97 forested versus open areas). In the context of herbivore species, $\delta^{13}\text{C}_{\text{ap}}$ values are influenced by the
98 photosynthetic pathway of consumed plants, enabling differentiation among C3, C4, and Crassulacean
99 Acid Metabolism (CAM) metabolic pathways (Koch et al., 2007).

100 The recent development of high-resolution micro-XRF (μXRF) line scanning to analyze trace element
101 abundances on cleaned surfaces of mammal molars serves as a valuable complement to conventional
102 isotope proxies (de Winter et al., 2019; de Winter and Claeys, 2016). The findings demonstrate a link
103 between seasonal fluctuations and trace element patterns in enamel, namely in Sr/Ca, Zn/Ca, K/Ca,
104 Fe/Ca and S/Ca. These ratios reflect the intake of trace elements through dust (discerning between
105 summer and winter) or dietary modifications. The documented connection constitutes a promising
106 avenue for utilizing these trace element ratios as a novel proxy to explore seasonal fluctuations in both
107 the ancient environment and dietary habits of extinct Proboscideans, potentially applicable to other
108 mammalian species (de Winter et al., 2017; Kohn and Cerling, 2002) .

109 Tooth enamel is regarded as one of the most diagenetically inert biominerals and its chemical and
110 isotopic compositions are preferred paleoenvironmental and paleoclimatic proxies (Forbes et al., 2010;
111 Fricke and O'Neil, 1996; Kohn, 1996; Kohn and Cerling, 2002). During precipitation, enamel biomineral
112 composition not only respond to the local chemical environment, i.e. the bioavailability of chemical
113 elements, but also to physiological and taxonomical characteristics. The latter is clear from species-
114 specific variations in biomineral composition in taxa that occur in the same environment (Kohn et al.,
115 2013). Therefore, our research design comparing related proboscidean taxa aims to isolate climatic and
116 environmental information from the chemical composition of the bioapatite samples.

117 The nano- to microcrystalline structure of tooth bioapatite has several sites for cations and anions,
118 which permit the uptake of a variety of elements with rather different chemical features. These
119 elements find their way from the environment into plant and animal tissue, including bone and tooth
120 material. For this reason, the chemical and isotopic composition of bioapatite became an important
121 tool to monitor climatic and ecological change (Kohn and Cerling, 2002; Macfadden et al., 1999; Tütken
122 et al., 2007). The bioapatite mineral lattice can accommodate iso- and heterovalent substitutions
123 during life or diagenesis varying its chemical composition through (geological) time, making bioapatite
124 a unique archive of physical and chemical information for both the living cycle and the events occurring
125 after death (Malferrari et al., 2019).

126

127

128 1.3 Proboscidean teeth as archives for terrestrial environmental variability and paleobiology

129 Mammal tooth enamel has emerged as a valuable recorder of paleo-seasonality due to its resistance
130 to diagenesis and its sequential growth, facilitating the retrieval of records with exceptional temporal
131 resolution (Blaise and Balasse, 2011). An additional benefit of employing mammal teeth for sub-annual
132 environmental reconstructions is the potential to amalgamate several teeth from a single individual,
133 forming a composite time series. This combination enables the generation of extended, uninterrupted
134 records depicting fluctuations in paleoenvironmental conditions throughout the years when the teeth
135 underwent mineralization (De Winter et al., 2016; Kohn and Cerling, 2002).

136 Proboscideans, which are among the largest land herbivores of the Neogene era (Fig. 1A), are
137 polyphyodonts, undergoing cycles of tooth replacement over their lifetimes (Lee et al., 2012). New
138 teeth gradually develop at the rear of the mouth, moving forward to displace and replace the anteriorly
139 located older ones (molar progression; Fig. 1B) (Lee et al., 2012; Metcalfe and Longstaffe, 2012). Their
140 molars are lophodont (Fig. 1C and D), composed of enamel lophs filled with dentin and surrounded by

141 cementum (Lee et al., 2012). Throughout the process of tooth formation, the growth of enamel initiates
142 at the front of the crown and advances in a loph-by-loph manner towards the distal end of the tooth
143 and the root. This progression continues until it reaches the point where the crown and root meet,
144 offering a distinct pathway for conducting analyses of seasonality (Fig. 1). The rates at which enamel
145 accumulates in proboscidean molars suggest the possibility of capturing an environmental record
146 spanning up to 15 years (Metcalf and Longstaffe, 2012), with an enamel accretion rate up to
147 ~13 mm/yr (Dirks et al., 2012; Esker et al., 2019; Kowalik et al., 2023). Accordingly, research on enamel
148 accretion rate (Dirks et al., 2012; Esker et al., 2019; Kowalik et al., 2023; Metcalf and Longstaffe, 2012),
149 confirms the possibility of capturing an environmental record spanning up to 15 years (Dirks et al.,
150 2012). Nevertheless, since molars are worn during feeding, selectively removing the older parts of the
151 record, this span can significantly decrease (see examples illustrating such difference in Fig.3 A and C)
152 (Esker et al., 2019). Ultimately, the time captured in a single tooth is governed primarily by enamel
153 extension rate and crown formation time (Kowalik et al., 2023). Crown height plays a secondary role,
154 because wear can remove large portions of the developmental sequence regardless of morphology
155 (Kowalik et al., 2023). Thus, low-crowned gomphothere molars may capture a shorter interval only if
156 their enamel grew more slowly or if wear removed a larger proportion of the crown (Metcalf and
157 Longstaffe, 2012). Based on the previous, in realistic terms for a low-crowned gomphothere molar
158 (where preserved enamel lengths are often on the lower side, say ~30–80 mm), one should expect on
159 the order of ~2–8 (up to ~15) years of record in many cases (Kowalik et al., 2023). Records of up to ~15
160 years are plausible if the enamel is worn slowly and accretion rate is high. But short (a few years) is
161 equally plausible if crown height is low or teeth are heavily worn.

162 Proboscideans possess a diverse evolutionary lineage and extensive fossil record, rendering them a
163 captivating subject of study. This characteristic offers the potential for terrestrial paleoclimate
164 reconstruction, spanning from the Late Paleocene era to the present day (Cantalapiedra et al., 2021;
165 Liu et al., 2008).

166

167 1.4 *G. angustidens* and modern elephant evolution and biogeography

168 *Gomphotherium* (Fig. 1A) is an extinct genus of gomphothere proboscidean, which once roamed the
169 Neogene landscapes of Eurasia, Africa, and North America (Wang et al., 2014). Its origin can be traced
170 back to Africa during the late Oligocene to early Miocene period (Wang et al., 2017). The earliest fossils
171 of *Gomphotherium*, date back approximately 19.5 million years, and were discovered in Africa (Wang
172 et al., 2017). Around 19 million years ago, *Gomphotherium* embarked on a range shift into Eurasia via
173 the "*Gomphotherium* Land Bridge", a land bridge that connected Eurasia to Afro-Arabia (Harzhauser et
174 al., 2007). Upon its arrival in Eurasia, *Gomphotherium* experienced rapid evolutionary changes,
175 reaching its zenith of diversity during the Early-Middle Miocene epoch. As the Pliocene dawned, the
176 last known *Gomphotherium* species vanished from North America, around 5 million years ago
177 (MacFadden et al., 2015).

178 Most *Gomphotherium* species reached a size comparable to the modern Asian elephant. They were
179 characterized by their distinctive long lower jaw tusks and four-tusked dentition (Larramendi, 2015).
180 Gomphotheres inhabited a diverse range of habitats, and while the majority of *Gomphotherium* species
181 are believed to have been browsers, indications suggest that certain specimens of *G. steinheimense*
182 from China showed grazing habits (Wu et al., 2018). Modern elephants are primarily considered
183 browsers, rather than grazers, although they do consume grasses as part of their diet, especially during
184 times of food scarcity (Wu et al., 2018).

185 The evolution of elephantids is believed to have stemmed from gomphotheres, and the forebears of
186 modern elephants might be African members of the "tetralophodont gomphothere" *Tetralophodon*
187 (Geraads et al., 2019). The family's earliest members date back to the Late Miocene period,
188 approximately 9-10 million years ago (Saegusa et al., 2014). While early members of Elephantidae had

189 lower tusks, these were lost in later members as the feeding function of the mandible shifted gradually
190 to the trunk, possibly as an adaptation to slightly more grazing habits (Li et al., 2023; Mothé et al.,
191 2016). By the end of the Miocene epoch, elephants and mammoths diverged from each other, and
192 during the Pliocene the elephantid range shift from Africa started, leading to the arrival of mammoths
193 and *Elephas* in Eurasia approximately 3.8-3 million years ago (Iannucci and Sardella, 2023).

194 One critical aspect of proboscidean evolution was the modification of their cheek teeth occlusal
195 morphology, which changed from the low-crowned bunolophodont molars of the trilophodont
196 *Gomphotherium* with few lophs, to the high-crowned and multi-plated teeth of the more derived
197 elephantiforms such as *Loxodonta* (Wu et al., 2018). This evolution is relevant because such dental
198 change allowed them to consume more abrasive foods with the spread of C4 vegetation between 8 to
199 5 Ma (Wu et al., 2018). While these changes in the morphological and ecological context may cause
200 some differences in the composition of teeth from extant and the extinct specimens, comparison
201 between modern elephants and the Middle Miocene *Gomphotherium* still contributes to our
202 understanding of how modern elephants and their ancestors adapted and diversified over the last
203 millions of years.

204

205 1.5 *Gomphotherium* dietary and environmental changes in Middle Miocene climate

206 This study presents a comparison between seasonal patterns in trace element concentrations of and
207 extant elephants and extinct Middle Miocene *Gomphotherium*. The Miocene record in Portugal
208 provides favourable conditions for conducting this research on fossil *Gomphotherium* specimens
209 (Antunes and Pais, 1984; Pais et al., 2012), since it is supported by a robust stratigraphic framework
210 and detailed depositional sequences, biostratigraphy and isotopic dating based on marine fossils, while
211 also exhibiting a substantial connection with terrestrial sedimentary formations.

212 The Middle Miocene *G. angustidens* material described here was collected in Portugal (Lisbon region;
213 Fig. 2A B and C). In this region, this species lived prior to the major ecological expansion of C4 biomass
214 between ~8 and 5 million years ago (Cerling et al., 1997a), and before the emergence of Elephantidae
215 from the ancestral stock of Miocene gomphotheres (Cerling and Harris, 1999). This temporal division
216 coincides with the Middle Miocene Climatic Optimum (MMCO), that occurred approximately 14 to 17
217 million years ago. During this period, the Earth experienced relatively warmer and more stable climatic
218 conditions, with higher temperatures than immediately before or after this interval. The MMCO was
219 characterized by reduced polar ice and relatively uniform temperatures across latitudes, making it a
220 period of significant climatic stability during the Miocene epoch (Westerhold et al., 2020; Zachos et al.,
221 2001).

222 Climatic assessments based on marine samples from the Middle Miocene of the Lower Tagus Basin
223 (LTB) indicate prevailing tropical conditions in the studied region (Pais et al., 2012). During the Upper
224 Burdigalian and Langhian stages (~17 – 15 Ma), water temperatures reached a peak (Pais et al., 2012),
225 resembling the present-day climate of the Guinea Gulf, classified as tropical monsoon climate (Köppen
226 classification “Am”) characterized by high temperatures, high humidity, and heavy rainfall year-round,
227 driven by the Intertropical Convergence Zone (ITCZ) and the West African monsoon. Sampling sites
228 were adjacent to coastline areas, as Miocene paleogeography for the Iberian Peninsula was very similar
229 to modern configuration, as recently documented by (He et al., 2023). (Pais et al., 2012).

230

231 2. Materials

232 2.1 *Gomphotherium angustidens*

233 Insights into continental Miocene landscapes are derived from the analysis of molars, representing the
234 extinct proboscidean. The selected *G. angustidens* specimens were collected at Quinta da Farinheira,

235 Chelas Valley (Fig. 2B), falling within the Cotter (1956) subdivision Vb, and the subdivision SDL1 (
236 (~15.9–16.1 million years ago (Antunes and Ginsburg, 2003). It belongs to the Middle Miocene
237 Langhian stage and the MN5 biozone and the final part of MN4 (13.7–16.0 Ma; Fig. 2C). The encasing
238 friable reddish terrigenous material presents reddish hues (Fig. 2D and E) provides ideal conditions to
239 extract the molars of interest without risking mechanical damage. This subdivision includes the
240 Burdigalian and Langhian stages (Pais et al., 2012). The specimens are curated at the Department of
241 Earth Sciences of the Universidade NOVA de Lisboa and are molars accessioned with the numbers: FCT-
242 DCT-4943, FCT-DCT-4944, and FCT-DCT-4945 (Fig. 3A to C and Fig. 4). The presence of juvenile molars
243 can be ruled out based on several independent indicators. First, the teeth show fully developed crown
244 morphology and plate count appropriate for adult stages; juvenile gomphotheres have fewer lamellae,
245 reduced crown height, and incomplete enamel formation (Shoshani and Tassy, 1996). Second, the wear
246 facets indicate sustained adult mastication rather than the light or uneven wear typical of juveniles.
247 Third, the dimensions of the preserved molars fall within adult size ranges for the taxon (Shoshani and
248 Tassy, 1996). Taken together, these features are incompatible with a juvenile ontogenetic stage, so
249 juvenile bias does not affect our geochemical interpretations.

250

251

252 2.2 *Loxodonta africana*

253 The extant proboscidean analogue material belongs to the African elephant *Loxodonta africana*. It was
254 provided by Jardim Zoológico de Lisboa (Lisbon Zoo) and consists of a complete molar tooth (Fig. 3D
255 and Fig. 4) also deposited at the Department of Earth Sciences of the Universidade NOVA de Lisboa
256 (FCT-DCT-4946). It belongs to an adult individual, born in the wild and later moved into an enclosed
257 environment in the Lisbon Zoo until its death, at the end of the 20th century. It is not uncommon to
258 find fallen elephant molars amongst hay and other materials during cleaning activities at the Zoo. This
259 is the case of the sample used in this study, accounting for the uncertainty regarding to which individual
260 they belonged to, as well as if the molar was mineralized in the wild or during captivity. Since a few
261 decades, the Lisbon Zoo shelters African elephants born and raised in the wild as well as others born
262 under their care, a clear reflection of their reproductive success under optimum conditions. Animal
263 enrichment includes (among many others) a tight control on substrate (soil) composition, requiring
264 periodic addition of external components from variable sources to stimulate natural behaviours.

265

266 3. Methods

267 3.1 Sample preparation

268 Three molars, likely of different adult individuals, of *G. angustidens* (FCT-DCT 4943, FCT- DCT 4944 and
269 FCT-DCT 4945) and one molar of *L. africanus* (FCT-DCT 4946)(examples in Fig. 3 and 4) were cut in
270 mesio-distal (anterior-posterior) direction, perpendicular to the orientation of the lophs in *L. africana*
271 and the cusp rows in *G. angustidens*, to reveal a cross section through the cusps of the molars (following
272 (Uno et al., 2020)). Cross sections were polished using CeO₂ powder suspension to ensure a flat surface
273 for μ XRF scanning (Fig. 4). Sectioning through the molars, while destructive, targeted the enamel in the
274 cusps/lophs using μ XRF line scanning to obtain time series of trace element composition through the
275 teeth (see **section 3.4**). The low number of individuals represented here could eventually present
276 limitations to our conclusions. Although our sample comprises only three gomphothere molars and
277 one modern elephant molar, these specimens are exceptionally rare and well-preserved, providing
278 high-resolution geochemical records that are otherwise unavailable for these taxa. So, even a small
279 number of teeth can yield meaningful insights into long-term dietary patterns and environmental
280 conditions, particularly when each tooth captures several years of enamel formation. The scarcity of
281 such material underscores the significance of these analyses for understanding proboscidean
282 paleoecology.

283
284
285
286
287
288
289
290
291
292
293
294
295
296
297
298
299
300
301
302
303
304
305
306
307
308
309
310
311
312
313
314
315
316
317
318
319
320
321
322
323
324
325
326
327
328
329
330

3.2 Mineralogical analysis of soil samples

To characterize the chemical components of soil potentially contributing to the composition of the molar enamel during mineralization and/or diagenetic evolution, the mineralogical composition of soil samples associated with both modern and fossil molars used in this study was analysed. Samples were taken from sediment material found directly around the selected molar 4943 and inside the cavities between the cusps. In samples associated with modern elephant models, soil particles were isolated from the organic matter in material lodged between the molar cusps by soaking samples in deionized water and decanting the liquid and floating constituents from the samples. In this way, only soil particles were taken into account for further analysis. Sediment samples associated with fossil and modern molars were analysed using X-Ray Diffraction (XRD) with Cu-K α radiation, carried out using PANALYTICAL Phillips X'Pert PW3040/60 equipment, with the X'Pert 2.0 and Profit software (Department of Geosciences, University of Aveiro, Portugal). Scans were run between 4 and 65° 2 θ for bulk samples and between 2 and 40° 2 θ of non-oriented powder mounts of fine fractions for clay mineral identification. Divergence slit was fixed at 1.0, receiving slit at 0.20; the scan step size of 0.02 for 3050 points at continuous scan; time per step was 1 sec/2 θ . Fine fraction analysis was carried out in the air-dry state and after glycerol saturation and heat treatment (500°C). Peak identification and semi-quantitative estimation were performed using HighScore software (Malvern Panalytical v. 4.9; ICDD database-International Centre for Diffraction Data). Identification of the different mineral phases followed the criteria recommended by (Brown and Brindley, 1980; Schultz, 1964) and the Joint Committee for Powder Diffraction Standards. Semi-quantitative mineralogical analyses followed the criteria recommended by (Mellinger, 1979; Schultz, 1964; Thorez, 1976); peak areas of the specific reflections were calculated and weighted by empirically estimated factors, according to (Galhano et al., 1999; Oliveira et al., 2002).

3.3 Trace element maps and profiles

3.3.1 Instrument setup

Concentrations of Ca, P, Na, Mg, Sr, S, Si, Fe, Al, K and Mn are determined across sections through proboscidean molars using an energy-dispersive Bruker M4 Tornado μ XRF scanner (Bruker nano GmbH, Berlin, Germany) at AMGC in Brussels. The XRF spectra produced enable detection and quantification of a wide array of elements (see (de Winter and Claeys, 2016)), however, the discussion is limited to the selected elements referred above. This selection was based on the degree of significance during elemental data processing (details in Appendix). We first mapped the entire cross section of each specimen using semi-quantitative mapping to identify the best-preserved areas in the fossil teeth by comparison between fossil and modern specimens. Then, we targeted those well-preserved enamel sections using quantitative elemental profiling (examples in Fig. 5).

The Bruker M4 Tornado features a Rh-anode X-ray source operated at 50 mV and 600 μ A (30 W) and two 30 mm² silicon drift detectors mounted in a low vacuum (20 mbar) chamber under a precise orientation such that the incoming and outgoing (detected) X-ray radiation describe a 90° angle when they hit the sample (see (de Winter and Claeys, 2016)). The X-rays from the source are focused using a poly-capillary lens. This configuration ensures that exciting X-rays can be focused on a round ~25 μ m diameter spot on the polished sample surface (calibrated for Mo-k α radiation), which is mounted on a XYZ moving stage to allow collection of a spatial array of XRF spectra. Peaks in XRF spectra belonging to elements of interest are identified and integrated using Bruker Esprit software, which includes a deconvolution algorithm for estimating the relative contributions of overlapping peaks in the XRF spectrum.

331 3.3.2 μ XRF mapping

332 The entire surface of all cross sections is mapped using μ XRF to produce semi-quantitative maps of
333 trace element distribution. For μ XRF maps, the X-ray source is moved along the sample surface
334 continuously in a raster pattern while XRF spectra accumulate in 25 μm by 25 μm pixels with a total
335 integration time of 1 ms (following (de Winter and Claeys, 2016). This sampling strategy does not allow
336 enough integration time for spectrum-by-spectrum quantification of trace element concentrations, but
337 instead produces semi-quantitative element distribution maps by creating false-colour images of the
338 deconvoluted surface area under element peaks (Fig. 5 and
339 <https://doi.org/10.5281/zenodo.14882824>). These maps were not used to determine accurate
340 concentrations of elements in the specimens, but used to guide the optimal location for quantitative
341 XRF line scanning.

342

343 3.3.3 μ XRF line scanning

344 Quantitative μ XRF trace element profiles are measured along the exposed enamel in cross sections
345 through the cusps and lophs of the proboscidean molars (see Fig. 3). We apply point-by-point line
346 scanning (following (Vansteenberghe et al., 2020), allowing the detectors to count fluorescent X-rays
347 returning from the sample for 60 seconds per point (following (de Winter and Claeys, 2016). This
348 approach allows enough measurement time per point to reach the Time of Stable Accuracy and Time
349 of Stable Reproducibility recommended in (de Winter et al., 2017), thereby achieving a compromise
350 between spectrum quality, measurement time and spatial resolution of the trace element profiles.
351 Trace element concentrations are quantified using the matrix-matched bioapatite calibration
352 developed in (De Winter et al., 2016) using a combination of in-house and certified bioapatite
353 standards. This method achieves measurement errors better than 10% for all elements considered in
354 this study (see detailed error analysis in (de Winter and Claeys, 2016).

355

356 3.4 Stable isotope analyses

357 After carrying out the μ XRF analyses, enamel samples were drilled using a hand-held dental drill
358 (Dremel equipped with a 3 mm drill-bit) from the cross sections through the molars for stable carbon
359 ($\delta^{13}\text{C}$) and oxygen ($\delta^{18}\text{O}$) isotope analyses of the structurally bound carbonate in the tooth bioapatite,
360 performed at Universidade da Coruña (A Coruña, Spain). Bioapatite samples (N = 42) were drilled from
361 multiple parallel cusps and various heights along the cusps within the molars to quantify inter-tooth
362 variability in isotopic composition. Approximately 1 mg of enamel powder was used for stable isotope
363 analyses. No chemical pre-treatment was applied because samples were taken from freshly exposed
364 enamel surfaces obtained by cutting clean cross sections through the molars. These internal enamel
365 portions are unlikely to have been affected by surface contamination or post-depositional fluid
366 interaction. In addition, the taphonomic context of the site (see Section 2) indicates limited exposure
367 to diagenetic fluids, reducing the likelihood of secondary geochemical overprinting. Under such
368 conditions, previous studies have shown that untreated enamel can preserve primary biogenic signals,
369 and pre-treatment may unnecessarily risk modifying original isotopic or elemental compositions
370 (Spencer et al., 2024). Therefore, the risk of introducing diagenetic (labile) carbonate fractions in the
371 samples was sufficiently low to motivate the choice not to use pre-treatment techniques, which have
372 been demonstrated to affect the original isotopic composition of enamel in some cases (Pellegrini and
373 Snoeck, 2016; Wood et al., 2021). The carbonate was extracted following the protocol by (De Winter et
374 al., 2016). Extracted carbonate samples were reacted with 99% orthophosphoric acid ($\text{H}_3\text{PO}_4 + \text{H}_4\text{P}_2\text{O}_7$)
375 in a carbonate preparation device (GasBench II, by ThermoFinnigan) to produce CO_2 , which is purified
376 using a series of condensation traps before being led into an isotope-ratio mass spectrometer (MAT253,
377 by ThermoFinnigan) through a dual inlet interface. Stable isotope ratios were calculated from the ratios
378 of CO_2 masses 44, 45 and 46 analysed by the mass spectrometer and converted to delta values with
379 reference to the international Vienna Pee Dee Belemnite (‰VPDB) scale using the standards NBS19,

380 NBS18, CO-8 and LSVEC (IAEA, Vienna, Austria). Stable isotope results were determined to be
381 reproducible with a standard deviation less than 0.2 ‰ based on repeated measurements of Carrara
382 marble powder. To compare our enamel-bound stable oxygen isotope results with modern and
383 Miocene water oxygen isotope values obtained in previous studies, we used the enamel-water
384 conversion formula for large, water-dependent herbivores from (Hoppe, 2006) and we aligned the
385 VSMOW to VPDB scale using the formula in (Coplen et al., 1983), following the methodology in (de
386 Rooij et al., 2022) and (Wooller et al., 2021).

387

388 4. Results and interpretation

389 4.1 Mineralogical characterization of sediments associated with studied molars

390 The X-ray diffraction analyses on Mid-Miocene soil samples revealed quartz as the main constituent
391 (*ca.* 95%; Table 1). Samples extracted from areas surrounding the teeth (inside and around) show lower
392 abundance of quartz (absent or 21 to 67%; Table 1) accompanied by a significant contribution of iron-
393 rich minerals (goethite, siderite, ilmenite). In contrast, modern sediment samples representing the host
394 substrate of the Lisbon Zoo are composed of approximately equal amounts of quartz and calcite (52
395 and 48%, respectively; Table 1). Calcite is not significantly present at any sample retrieved from Mid-
396 Miocene materials. Mid-Miocene sediment samples correspond to detrital quartz-grain deposits,
397 cemented into hard iron-rich crusts encasing the studied molars. Such “induration” is common in semi-
398 arid regions because of epidiagenetic processes (*sensu* (Staunton and Fairbridge, 2008), typically found
399 in flood plain alluvium, lacustrine and littoral deposits affected by strong seasonality: wet season leads
400 to dissolution and the dry season to capillary action and evaporation (Beauvais and Colin, 1993;
401 Staunton and Fairbridge, 2008). The presence of dolomite and/or gypsum (see Table 1) is also
402 consistent with strong evaporation scenario (Díaz-Hernández et al., 2013). In contrast, the sediments
403 associated with the modern elephant molar show no evidence of such evaporation processes.

404 Clay mineral fractions also provided clear differences between Mid-Miocene and modern samples (Fig.
405 3): In ancient samples only illite was detected, whilst the modern sample is also dominated by illite
406 (84%) but also contains a small amount of smectite (16%; Fig. 6). Nevertheless, these differences may
407 be considered as negligible in terms of original composition of the ancient clay assemblage for two
408 reasons: (i) Smectite decays readily under shallow burial conditions (illitization of smectite) as water is
409 expelled from the interlayer space and sheets become more and more organized, leading to a well
410 crystallized illite crystal structure (Kübler and Jaboyedoff, 2000). It is thus plausible that smectite was a
411 part of the initial composition of the clay assemblage of mid-Miocene soils, as seen for the modern soil
412 sample (Fig. 6). (ii) Sediments reflecting a clay mineral composition of 100% illite are highly uncommon
413 (Journet et al., 2014), corroborating the probable illitization of original smectite. Therefore, the original
414 clay mineral assemblage at both sites can be considered similar, but further comparisons are limited,
415 as soil substrate at the Lisbon Zoo may not necessarily reflect local sediment composition (as described
416 in section 2.2).

417

418 4.2. Stable carbon and oxygen isotope composition of tooth enamel bioapatite

419 Mid-Miocene molar samples present $\delta^{13}\text{C}$ values between -9.2 and -9.9‰VPDB (mean value \pm standard
420 deviation (s.d.) = $-9.7 \pm 0.3\%$ VPDB; Fig. 7), in clear contrast with the modern elephant molars, whose
421 values range from -11.9 to -13.2‰VPDB (mean \pm s.d. = $-12.8 \pm 0.3\%$ VPDB). Differences in $\delta^{18}\text{O}$ are also
422 clear, with Mid-Miocene samples clustering between -1.7 and -6.7‰VPDB (mean \pm s.d. = $-3.5 \pm$
423 1.0% VPDB) and modern samples between -7.9 and -11.1‰VPDB (mean \pm s.d. = $-8.6 \pm 0.7\%$ VPDB). The
424 extent of diagenetic alteration can be evaluated by assessing the degree of isotopic heterogeneity
425 and/or homogeneity among specimens from a single deposit (Kohn and Cerling, 2002). In this way, the
426 observed clustering of all Mid-Miocene samples against the tight cluster formed by the modern molar
427 samples is taken as evidence of fair preservation of the older molars. This interpretation is further

428 validated by contrast with available literature for coeval materials and (paleo) environmental
429 conditions deduced for the factors controlling the obtained isotopic differences. When compared with
430 previous studies, we find that both our modern and our *Gomphotherium* $\delta^{13}\text{C}$ data aligns well with
431 previous $\delta^{13}\text{C}$ measurements for these taxa. The $\delta^{18}\text{O}$ values measured in *Gomphotherium* for this
432 study are high compared to most literature $\delta^{18}\text{O}$ values of the same genus, while our modern elephant
433 $\delta^{18}\text{O}$ values are slightly lower than those of other modern and Pleistocene elephants (Figure 7).

434

435 4.3 Elemental composition of molar enamel

436 Semi-quantitative XRF maps highlight the distribution of multiple elements throughout the tooth
437 specimens (see elemental maps in <https://doi.org/10.5281/zenodo.14882824>). The maps show clear
438 features elevated in the concentrations of elements such as Fe (example in Fig. 5), which indicate patina
439 or encrustation on the outside of the teeth or cracks in the teeth which are enriched in these detrital
440 elements. The cementum cavity and dentine are also enriched in these elements compared to the
441 enamel layers. These areas were avoided as much as possible during line scanning to exclude the
442 influence of these postmortem processes from our interpretation. Outside these clearly diagenetic
443 features, the enamel of the *G. angustidens* specimens studied here is broadly similar to that of the
444 modern elephant, and to that of previous other modern mammal tooth enamel (De Winter et al., 2016;
445 Kohn, 2008) attesting to its preservation and lack of diagenetic alteration.

446 A summary of mean elemental values obtained for selected elements (Ca, P, Na, Mg, Sr, S, Si, Fe, Al, K
447 and Mn) based on quantitative XRF line scans is shown in Table 2 and Figure 8. Because of a wide array
448 of expected differences amongst the studied molars (geological age, geographical origin, taxonomic
449 difference), overall discrepancies in absolute values are beyond the scope of this contribution. Yet, due
450 to the potential interaction with surrounding soil and diagenetic incorporation of Si, Fe, Al, K (e.g.,
451 Białas et al., 2021; Brüggmann et al., 2012), the fact that these elements show no clear enrichment
452 trend when comparing modern with ancient values seems to point towards a fair preservation of the
453 elemental composition of Mid-Miocene molars (see Table 2).

454

455 Iron is the only exception, but likely because Miocene molars are encased on iron-rich crusts (section
456 4.1). If iron oxide encrustation caused elevated Fe in the fossil specimen, such enrichment should be
457 higher on the outside of the molars, a pattern visible in the line scan results (see below) and the XRF
458 maps (see Appendix; <https://doi.org/10.5281/zenodo.14882824>). In this case, elemental fluctuations
459 observed in phase with Fe are suspect of diagenetic influence and not interpreted in the discussion.
460 Since diagenetic alteration can lead to depletion or enrichment of some elements (Fig. 8 and Table 2),
461 we focus on discussing elemental trends and associations (rather than absolute abundance), as these
462 features may enclose (paleo) environmental fluctuations during the growing period (typically <4/5years
463 (Uno et al., 2020).

464

465 Elemental associations were obtained by performing Principal Component Analysis (PCA) on Mid-
466 Miocene and modern elemental data (Fig. 9). Details on preliminary data treatment and exploratory
467 analysis are provided in Supplementary File (Figs. S1 to S4). Principal Component Analysis has been
468 shown to help detecting diagenetic signatures in fossil archives, because elements associated with
469 diagenetic alteration (e.g. Mn and Fe in the case of carbonates (Ullmann and Korte, 2015) or rare earth
470 elements, U and Mn and Fe in the case of bioapatite (de Winter et al., 2019; Kohn, 2008; McMillan et
471 al., 2019) tend to cluster into a clearly distinguishable principle axis due to their strong enrichment in
472 altered parts of the fossils (Coimbra et al., 2020). Modern and ancient samples provided very similar
473 PCA loading plots (Fig. 9A and B). Principle Component 1 (PC1) is characterized by an opposing trend
474 of Ca and P concentrations on the one hand against concentrations of Fe, Si, Al, K (with minor
475 contributions of Mn and Sr) on the other. Principle Component 2 (PC2) represents a trend of Ca and P

476 concentrations contrasted to samples with higher Na, Mg and Sr concentrations. Accordingly, lowered
477 Ca and P values are associated to increased abundance of the remaining elements (“closed sum effect”;
478 Fig. 9A and B), but without relation between the groups of elements separated in different components
479 (PC1: Fe, Si, Al, K; PC2: Na, Mg, Sr). Sample distribution along the PCA score plots (Fig. 9C and D) shows
480 a main cluster from which a small number of samples deviate towards higher concentration of Fe, Si,
481 Al, K (negative PC1 values; horizontal axis) and higher concentration of Na, Mg, Sr (positive PC2 values;
482 vertical axis). Because these elemental associations are seen in both modern and ancient samples,
483 diagenetic control on obtained elemental distributions is unlikely (also shown during exploratory data
484 analysis; Supplementary File). The observed cluster distribution suggests that incorporation of Fe, Si,
485 Al, K and Mn occurs only sporadically and may partly highlight incorporation of small fractions of
486 detrital matter on the edges of the line scans where they exit the enamel. In contrast, Na, Mg and Sr
487 incorporation is recurrent throughout the elemental dataset, suggesting consistent variability within
488 the enamel which may be linked to *in vivo* environmental variability recorded in the teeth (see (De
489 Winter et al., 2016).

490

491 The variability in concentrations of the statistically most relevant elements from each cluster
492 defined by PCA (Ca, Na, Fe and Si) along molar growth was tested by representing the fluctuations in
493 their abundance along the measured transects (Fig. 10). Along transects in growth direction through
494 modern elephant molars (Fig. 10A), Ca and Na show pronounced fluctuations, which are inversely
495 correlated. This relationship between Ca and Na is only rarely disrupted when Fe and Si concentrations
496 are conspicuously higher, in which case Ca and Na both decrease (Figure 10). The mid-Miocene
497 elemental transects reflect the same trend (Fig. 10B) with an anti-phase pattern of Ca and Na with
498 significant fluctuations within one single transect. Concentrations of Ca and Na jointly decrease in
499 locations where Fe and Si show sharp increases. The evolution of Fe and Na along the transects, which
500 sample the same part of the ontogenetic history in each molar were further compared to evaluate their
501 potential as seasonality archives (Figs. 11, 12 and 13). The resulting comparison shows that both
502 episodic increases in Fe concentration and periodic fluctuations in Ca and Na concentrations in the
503 modern elephant and Miocene *G. angustidens* molars are reproduced along parallel transects in the
504 same tooth.

505

506 5. Discussion

507

508 5.1 Stable isotope signatures in bioapatite

509 5.1.1 Feeding preferences derived from $\delta^{13}\text{C}$ signature in Mid-Miocene and modern molars

510 The stable carbon isotope composition ($\delta^{13}\text{C}$ value) of body tissue of extant herbivores reflects
511 the type of vegetation (C_3 vs. C_4) they consume. Terrestrial plants may follow three types of
512 photosynthetic pathways to fix CO_2 from the atmosphere: the C_4 , C_3 , CAM pathways (Bender, 1971;
513 Ehleringer et al., 1991; Farquhar et al., 1989). The C_3 and C_4 photosynthetic pathways exhibit different
514 $\delta^{13}\text{C}$ values, with most C_4 plants (tropical grasses and sedges) containing carbon with an isotopic value
515 between -10‰ and -15‰ VPDB and most C_3 plants (most trees, shrubs, or high-latitude grasses)
516 between -22‰ and -35‰ VPDB (Bender, 1971; Vogel, 1980). The distinct isotopic composition of C_3
517 and C_4 plants translates to a distinct isotopic signature in tooth enamel carbonate that can be used as
518 a proxy for browsing (mostly C_3) versus grazing (mostly C_4) diet of animals. The typical range of $\delta^{13}\text{C}$
519 values for these different feeding strategies shown in Fig. 7 to compare with our results were obtained
520 from (Cerling et al., 2003b, 2003a; Cerling and Harris, 1999; Clementz, 2012; Martínez del Rio and
521 Carleton, 2012). Metabolic pathways in an animal increase the $\delta^{13}\text{C}$ values by up to 14‰ in the dental
522 enamel apatite relative to plant tissue they consume (Cerling and Harris, 1999; Patnaik et al., 2019),
523 where body size can also be of relevance (Tejada-Lara et al., 2018). Further, animals feeding in closed
524 canopy forests have a lowered $\delta^{13}\text{C}$ composition compared to those feeding in more open woodland

525 environments due to the recycling of respired CO₂ (¹³C depleted) on the forest floor and low light
526 intensities at ground level that results in more negative δ¹³C values in plants (Cerling et al., 2004;
527 Patnaik et al., 2019; van der Merwe and Medina, 1991). For the present study, additional aspects are
528 of relevance. Indeed, δ¹³C values in modern elephant molars are expected to be ca. 1.5‰ lower relative
529 to Miocene *G. angustidens* values due to a shift in atmospheric δ¹³C since the Industrial Revolution and
530 fossil fuel combustion (Cerling et al., 1997b, p. 97; Passey and Cerling, 2002; Tipple et al., 2010).

531 The range of δ¹³C values obtained for Mid-Miocene samples largely overlaps the range
532 commonly reported for Mid to late-Miocene *Gomphotherium* samples from a variety of locations (Fox
533 and Fisher, 2004; Patnaik et al., 2019; Wu et al., 2018); Fig. 7). All reported values plot along the upper
534 extreme range for C₃ consumers (-8 to -12‰VPDB; Fig. 7), indicating that—also in Iberia—these
535 individuals foraged in partially open, possibly arid conditions, favouring woodlands as their preferred
536 habitat. Additionally, lack of evidence pointing towards of mixed-feeding preferences indicates that
537 western Iberian areas of woodland habitat could support these large-bodied herbivores through the
538 Mid-Miocene. In clear contrast, modern elephant δ¹³C values obtained in this study as well as from
539 other localities (Ma et al., 2019; Uno et al., 2020); Fig. 7) plot towards lower values (-10 to below -
540 14‰VPDB), within the range of closed canopy forest environments. Regarding the modern samples
541 used in this study, the obtained result suggests that the animal developed the molar in the wild, prior
542 to transport to its zoo environment.

543

544 5.1.2 Hydrological differences between Mid-Miocene and present-day environments

545 The δ¹⁸O of tooth enamel reflects the δ¹⁸O of ingested water, largely influenced by precipitation,
546 latitude, altitude, aridity, and evaporative processes, as well as physiological/behavioural water
547 conservation factors and metabolic processes of mammals (Kohn, 1996; Kohn et al., 1996, p. 96; Luz et
548 al., 1984). Obligate drinkers, such as elephants, frequently ingest water, which largely reflect rainfall
549 oxygen-isotope composition whilst more drought-tolerant non-obligate drinking mammals (e.g. *Oryx*)
550 are affected by evaporative enrichment of δ¹⁸O values (Ayliffe and Chivas, 1990; Kohn et al., 1996; Levin
551 et al., 2006; Roberts et al., 2018). Concomitantly, environmental temperature changes (e.g.,
552 seasonality) tend to lead to the enrichment of the δ¹⁸O signature in the water source in warmer
553 conditions and relative depletion in cooler conditions (Bryant et al., 1996). However, we acknowledge
554 that, besides temperature, (seasonal) fluctuations in humidity/aridity can also significantly influence
555 the δ¹⁸O of water bodies in terrestrial ecosystems (Luz et al., 1984). We therefore emphasize that this
556 proxy does not record a pure (seasonal) temperature signal.

557 The range of δ¹⁸O values obtained for Mid-Miocene molar samples is similar to the high end of the
558 range of δ¹⁸O values measured in North American Mid to Late-Miocene *Gomphotherium* molar samples
559 found in the literature ((Fox and Fisher, 2004); Fig. 7), but significantly higher (less depleted) than values
560 reported for Indian and Asian Mid-Miocene *Gomphotherium* molars ((Białas et al., 2021; Patnaik et al.,
561 2019; Wu et al., 2018); Fig. 7). Investigating the expected δ¹⁸O values of precipitation along these
562 different areas of the globe during the Miocene provides clues to explain these differences. The
563 obtained oxygen isotope values in the Mid-Miocene molar samples overlap almost exactly with δ¹⁸O
564 values modelled for rainfall during dry season in western Iberia during the Middle Miocene (Botsyun
565 et al., 2022). Similarly, oxygen isotope compositions in Asian *Gomphotherium* molars are also
566 compatible with pedogenic carbonate δ¹⁸O values from the Chinese Loess Plateau and northern
567 Pakistan, which record the isotopic value of local surface waters in these Asian region (Quade et al.,
568 1989; Wang et al., 2023). Considering this relationship, the comparison between δ¹⁸O values recorded
569 in modern and fossil molars reveals that Mid-Miocene weather in western Iberia was likely warmer
570 and/or less humid than in Asia during coeval times.

571 Comparing modern elephant enamel δ¹⁸O values and local precipitation values in SW Iberia generates
572 a significant discrepancy of ca. 5‰ (Fig. 7). Such a difference is not observed in other modern samples
573 (Fig. 7), which show a very consistent overlap in δ¹⁸O values between δ¹⁸O_{enamel} and δ¹⁸O_{precipitation}.

574 Therefore, as already suspected from the interpretation of $\delta^{13}\text{C}$ values, the modern elephant living at
575 the Lisbon Zoo is unlikely to have developed his molar in that locality, thus reflecting $\delta^{18}\text{O}$ values of the
576 original location in the wild. Based on considerably depleted $\delta^{18}\text{O}$ values (ca. -8.5‰), possible origins
577 of the modern specimen include central Angola, southern Democratic Republic of the Congo or Zambia,
578 where the more depleted range of surface water $\delta^{18}\text{O}$ values overlaps with $\delta^{18}\text{O}$ values of drinking
579 water expected based on the enamel- $\delta^{18}\text{O}$ values in our modern elephant specimen (“Water Isotopes
580 Database,” 2023). Due to limited documentation, we cannot know with certainty which elephant the
581 molar came from. Our best guess can be based on geochemical data and by comparing this data to
582 literature. Certainly, Lisbon water sources can be ruled out, so the search for potential origin may be
583 speculative, but still exciting to obtain so much information from the available dataset.

584 In summary, carbon and oxygen-isotope values obtained from Mid-Miocene molar samples
585 demonstrate an open-canopy woodland habitat preference for West Iberian *Gomphotherium*. Local
586 food supply sustained browsing communities even during dry season, as no evidence of grazing was
587 detected in $\delta^{13}\text{C}$ values. Therefore, warm and dry conditions seem to have prevailed in Western Iberia
588 during the Mid-Miocene. To isolate seasonal-scale variability in the paleoenvironment, high-resolution
589 elemental data are gathered and interpreted below.

590

591 **5.2 Elemental associations and chemical variability**

592

593 5.2.1 Differential incorporation of major and trace elements in molar enamel

594 The inorganic component of mineralized enamel is composed of 89% calcium hydroxyapatite
595 and small amounts of calcium carbonate, calcium fluoride and magnesium phosphate. Bioapatite in
596 enamel (and dentin) are deficient in calcium, rich in carbonates and prone to structural element
597 replacement (LeGeros, 1986). Ionic substitutions of enamel apatite (bioapatite) include Mg^{2+} , Na^+ ,
598 Mn^{2+} , Ni^{2+} , Cu^{2+} or Zn^{2+} for Ca^{2+} ; Cl^- or $\text{F}^-/\text{CO}_3^{2-}$ for OH^- ; and HPO_4^{2-} , CO_3^{2-} , AsO_4^{3-} , SO_4^{2-} for PO_4^{3-} (Sakae
599 et al., 1991; Sarna-Boś et al., 2022; Shaik et al., 2021). During lifetime, demineralization and
600 remineralization processes are constantly alternating on the surface of each tooth, also contributing to
601 potential changes in elemental composition of teeth (Nedoklan et al., 2021).

602 Magnesium is the most abundant Ca-substituting trace element in enamel, essential for the
603 proper development of the tooth structure (Sarna-Boś et al., 2022; Sharma et al., 2021). Magnesium
604 (and sodium) can replace Ca by ion exchange on the crystal surface during the secretion and maturation
605 of primary bioapatite. It may occur in a labile status, probably adsorbed onto the crystal surfaces (Aoba
606 et al., 1992a, 1992b). The elemental association obtained for both modern and ancient proboscidean
607 molars, which clearly show an inverse trend between Ca and P concentrations when compared to
608 abundances of Mg, Na and Sr (Fig. 9A and B), indicates that Ca replacement within enamel crystal
609 surfaces occurred naturally during molar development and/or during remineralization processes during
610 the animal’s lifetime. The fact that the largest cluster of samples is responding to this trend (Fig. 9C and
611 D) shows that this process is dominant over time, corresponding to tooth growth and later
612 maintenance stages, and not principally related to post-mortem diagenetic processes.

613 As observed by other authors, small amounts of externally incorporated elements (Si, Al, and
614 Fe, Mn and rare-earth elements) can also be found in fossil enamel, as long-term preservation of
615 bioapatite involves recrystallization and alteration processes, which drive enrichment of elements not
616 naturally abundant in unaltered enamel (Malferrari et al., 2019). Accordingly, minor enrichment or
617 depletion of key elements near the outer enamel rim may indicate the mobilization of these elements
618 into the bioapatite structure during diagenesis (see Fig. 5 for Fe; (de Winter et al., 2019; Kohn, 2008).
619 Conversely, lack of significant elemental changes in enamel Fe (and Mn) from the outer rim of the tooth
620 towards the innermost sections, as seen in our *Gomphotherium* specimens (see Fig. 11), denotes

621 inefficient impregnation of interstitial Fe- and Mn-oxides and oxyhydroxides (Kohn et al., 1999).
622 Additionally, lack of a clear difference in the elemental distribution between modern to fossil data is
623 typically taken as a good indicator that diagenesis had no significant influence on their distribution
624 (Białas et al., 2021). In conclusion, the following previously established lines of evidence for screening
625 for diagenetic influence on elemental enamel composition led us to conclude that our *G. angustidens*
626 dataset reliably records past dietary and environmental change:

- 627 1. Modern and ancient samples show similar elemental associations (Fig. 9A and B) and age-
628 dependent elemental enrichment in Fe, Si and Al is not observed (Table 2);
- 629 2. There is no clear pattern of trace element enrichment along the outer rims affecting the
630 locations of the selected transects (Fig. 10);
- 631 3. Only a small set of samples (13 and 17% of modern and ancient data; respectively) shows
632 elevated abundance of key elements associated with diagenetic alteration (as isolated in PC1;
633 Fig. 9C and D), showing this to be a sporadic enrichment events, rather than a pervasive
634 process.

635 Even at early diagenetic stages, local sedimentary factors influencing the mobilization of FeO,
636 F and SO₃, such as rock composition, pH value and redox potential, can control the introduction of
637 these elements into the tooth materials during fossilization. Similarly, comparable concentrations of
638 K₂O, SiO₂, and Al₂O₃ in both modern and fossil materials indicate that crystallization or mechanical
639 introduction of silicate phases into the fossil during diagenesis is of low importance. Therefore, even
640 elements typically attributed to early diagenetic evolution (Fe, Si, Al, K) can be interpreted to reflect *in*
641 *vivo* processes similar to the distribution of other major to minor elements (e.g., (Brügmann et al.,
642 2012). Short-lived periods of significant incorporation of Fe, Si, Al, K are inversely correlated to tooth
643 growth and maintenance processes evidenced by reduced Mg and Na fixation (Figs. 9 and 10). This is
644 taken as evidence of periods of environmental stress.

645

646 5.2.2. Elemental abundance in *Gomphotherium* molars reveals geophagic behaviour in ancient 647 proboscideans

648 The patterns of trace element concentration identified in the XRF line scans through the
649 *Gomphotherium* tooth enamel record differential elemental incorporation during the animal's lifetime.
650 Potential sources of elemental enrichment and causes leading to elemental depletion must be
651 interpreted in the light of natural behaviours carried out in response to environmental conditions
652 (Wheelock, 1980; Białas et al., 2021). Amongst these, geophagy is commonly observed in elephants.
653 Geophagy is defined as the deliberate and regular consumption of earthy materials such as soils, clays
654 or sediments by animals and humans (Abrahams and Parsons, 1996) and functions to supplement
655 dietary mineral deficiencies, alleviate gastrointestinal disorders or detoxify unpalatable foods
656 (Chandrajith et al., 2009; Holdø et al., 2002; Houston et al., 2001; Sach et al., 2019; Wheelock, 1980).
657 Soils consumed by African elephants were previously demonstrated to have higher Na⁺ concentrations
658 than the surrounding soils, hence deduced to be used to supplement an inadequate dietary-sodium
659 intake (Chandrajith et al., 2009; Wheelock, 1980). However, other possible roles of soil have also been
660 hypothesized as important in determining the extent of geophagy, including detoxification of plant
661 secondary compounds, countering the effects of acidosis (Houston et al., 2001). Mineral
662 supplementation is most likely not the sole factor driving geophagic behaviour (Holdø et al., 2002).

663 Further evidence for the relevance of geophagy and local sedimentary contexts in modern
664 elephants is deduced from the fact that soil used by elephants at Ngorongoro (North Tanzania) contains
665 ca. 35% kaolinite (Houston et al., 2001). Kaolinite, through its adsorptive ability, is effective in
666 neutralizing the activity of many plant secondary (toxic) compounds also serving as a barrier to protect
667 the gut lining from toxins in the food (e.g., tannins and alkaloids; (Sach et al., 2019). In this way, forest
668 elephants, which have access to kaolin soils, may be able to feed on a wider range of forest plant
669 species, which can be beneficial under nutritional stress resulting from low food quality during dry

670 season (Suba et al., 2016). Elephants purposefully select soils with high proportions of kaolinite and
671 illite, particularly during the dry season when food quality is relatively low (Chandrajith et al., 2009). In
672 this context, the clay assemblage recovered from both modern and ancient materials (Fig. 6),
673 dominated by illite $[KAl_2(Si_3, Al)O_{10}(OH)_2]$ and small contribution of smectite $[(Na,Ca)_{0,3}(Al,Fe,Mg)_2(Si,$
674 $Al)_4O_{10}(OH)_2 \cdot n(H_2O)]$ explains the incorporation of minor elements via geophagic behaviour, providing
675 a viable source of Fe, Si, K, Al (Figs. 9 and 10). Illite is reported to be the most abundant clay mineral in
676 land surfaces at a global scale (Ito and Wagai, 2017).

677 An alternative hypothesis explaining these spikes in Fe, Si and Al in our trace element profiles
678 could be the incorporation (either *in vivo* or postmortem) of fine-grained sediment into cracks in the
679 enamel. This would not require digestion of the minerals, but, if incorporated *in vivo*, would still point
680 to geophagic behaviour. After closely examining the distribution of these elements in XRF maps (Figure
681 10 and Appendix; <https://doi.org/10.5281/zenodo.14882824>) as well as the texture of the enamel at
682 the location of the XRF line scans, we consider this explanation unlikely, as no evidence of cracks in the
683 enamel is found at the measurement locations. This is a result of our measurement strategy, in which
684 we deliberately avoided these cracked areas when programming our XRF profiles (see **section 3.3.2**).

685 We hypothesize that the short-lived, sporadic increments in Fe, Si, Al in both modern and
686 ancient molars result from elemental incorporation due to geophagic behaviour during stressful, dry
687 season conditions. By comparing Fe trends along all measured transects (Fig. 11), it is possible to
688 identify the occurrence of several dry periods during molar growth (Fig. 11B, D, F and H). It is not
689 possible to confirm their seasonal periodicity with certainty here, as enamel growth rates cannot be
690 independently reconstructed, limiting the estimation of the amount of time comprised in each
691 transect. Tentatively, three to four dry seasons are identified based on the sharp Fe increments
692 coinciding with cyclical patterns in Na, suggesting that the obtained elemental archive recovers a period
693 of 3 to 4 years in the life of these animals. Based on the reasoning above, even small amounts of
694 externally incorporated elements (Fe, Si, Al) can serve as proxies to identify seasonality in modern and
695 ancient molar samples if the animals participated in seasonal geophagy. This result shows that Miocene
696 seasonality was sufficiently pronounced to have an impact on animal behaviour, stimulating geophagic
697 behaviour under seasonally stressful (warm and dry) conditions. Complementing these findings, Na
698 distribution likely indicates variations in tooth growth, with higher Na values highlighting growth under
699 optimal conditions (Fig. 12). The Na record showing smooth long-duration increments along one to
700 three periods (Fig. 12B, D, F and H) supports the interpretation that Na in our *Gomphotherium* can be
701 used as a proxy for seasonal changes in tooth growth rate, while the Fe spikes highlight periods of
702 drought, geophagy and reduced growth. This observation is supported by evidence of Na deficiency as
703 one of the drivers of geophagic behaviour and natural preference for Na-rich sediments (Chandrajith
704 et al., 2009; Wheelock, 1980). The timing of elemental signatures in the trace element records, which
705 reflect dry season, does not overlap with those interpreted to reflect more optimal growth conditions
706 (Fig. 13), which corroborates the usefulness of differential elemental incorporation as indicators of
707 seasonal variability in environmental conditions in ancient teeth. Based on these findings, the
708 applicability of trace elemental concentrations in well-preserved fossil enamel bioapatite as proxies
709 for geophagy behaviour and growth stress during past dry seasons is encouraging.

710

711 6. Conclusions

712 A combination of stable isotope and trace element analyses in molar enamel in Middle Miocene *G.*
713 *angustidens* from Western Iberia and modern *L. africana* from western Iberia reveals similar responses
714 of tooth bioapatite chemistry to episodic changes in the environment in both taxa. Based on stable
715 carbon and oxygen isotope composition in both taxa, Iberia was characterized by a warm and
716 seasonally dry climate during the Middle Miocene, and that *G. angustidens* thrived in an open-canopy
717 woodland ecosystem in this area. In contrast, the modern *L. africana* specimen developed his molar in
718 a Central African closed-canopy forest environment. Episodic increases in Fe and Si observed in trace

719 element profiles through *G. angustidens* molar enamel hint at geophagy behaviour during seasonally
720 dry and warm periods in this extinct taxon, behaviour patterns, which are also observed in modern *L.*
721 *africana*. Cross-validation via independent proxies suggests surrounding sediment as a probable source
722 of elemental enrichment, incorporated during molar development and/or during remineralization
723 processes. These results demonstrate the application of high-resolution (sub-seasonal scale) trace
724 element records through fossil teeth is critical to reconstruct the behaviour patterns of extinct
725 mammals in response to climate variability in their living environment.

726

727 **7. Acknowledgments**

728 RC acknowledges financial support from Geobiotec research Group (UIDB/04035/2020). MR thanks the
729 Stimulus of Scientific Employment, Individual Support – 2018 Call grant by the Fundação para a Ciência
730 e a Tecnologia (Portugal, CEECIND/02199/2018) and GeoBioTec as well as the Fundação para a Ciência
731 e a Tecnologia for the funding of the project 2021 EXPL/CTA-PAL/0832/2021 which directly
732 supports this research. DEL is recipient of a PhD grant funded by Fundação para a Ciência e a Tecnologia
733 (grant number 2020.05395.BD). RM is funded by Fundação para a Ciência e a Tecnologia (grant
734 number 2021.08458.BD). We also thank Micael Martinho and Carla Alexandra Tomás from the
735 preparation laboratory at GEAL-ML as well as Lígia Castro and Eduarda Ferreira from the Earth Sciences
736 Department at FCT-NOVA. Finally, a special thanks to the project manager Marlene Monte from
737 NOVA.ID.FCT. PC thanks Research Foundation Flanders (FWO) for purchasing μ XRF and VUB Strategic
738 Research for funding. NdW acknowledges financial support from the Flemish Research Council (FWO
739 postdoctoral fellowship; 12ZB220N and FWO Climate Prize) as well as the Dutch Research Council
740 (NWO) for his VENI fellowship (“MACRO”; VI.Veni.222.354).

741

742 **Data availability.** Supplementary data and figures belonging to this study were stored in the open-
743 source online repository Zenodo (<https://doi.org/10.5281/zenodo.14882824>)

744

745 **Author contributions.** RC, NdW, and MR conceived the work; all authors wrote, reviewed and edited
746 the manuscript. Samples were collected by MR, RB, DEL, PL and RM; laboratory procedures were
747 supervised and carried out by RC, NdW, MR and AG. FR and PC provided the framework, facilities and
748 necessary support to develop this research.

749

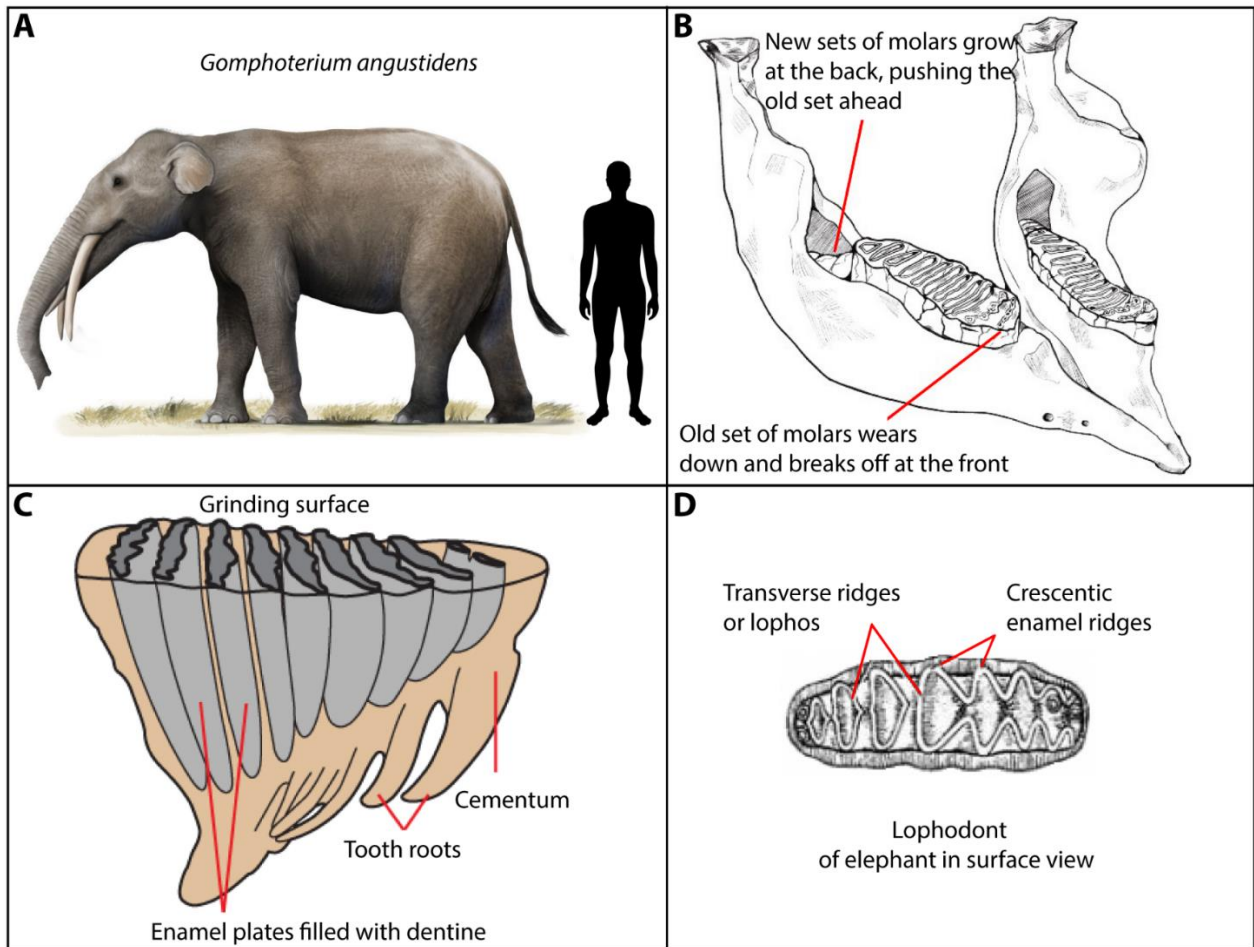
750 **Competing interest.** *Some authors are members of the editorial board of journal Biogeosciences.*

751

752 **Figure captions**

753

754 **Figure 1_Coimbra et al.**



755

756 **Figure 1.** Relevant aspects of Proboscidean morphology and dental anatomy. A) Artistic illustration of
757 *Gomphotherium angustidens* and scale relative to human silhouette (adapted from (“*Gomphotherium*
758 *angustidens* by cisiopurple on DeviantArt,” 2022), ©cisiopurple). B) Schematic representation of molar
759 growth process (adapted from (Jayachandran, 2022) ©Wildlife SOS). C) Molar structure and relative
760 distribution of enamel, dentine and cement (adapted from (“What Did Lupe Eat? - Mammoth
761 Discovery,” n.d.) ©Children’s Discovery Museum, San Jose, USA). E) Lophodont of elephant
762 in surface view, describing the intricate folding of enamel and dentine to form transverse ridges or lophos (adapted
763 from Bhavya, 2017).

764

765

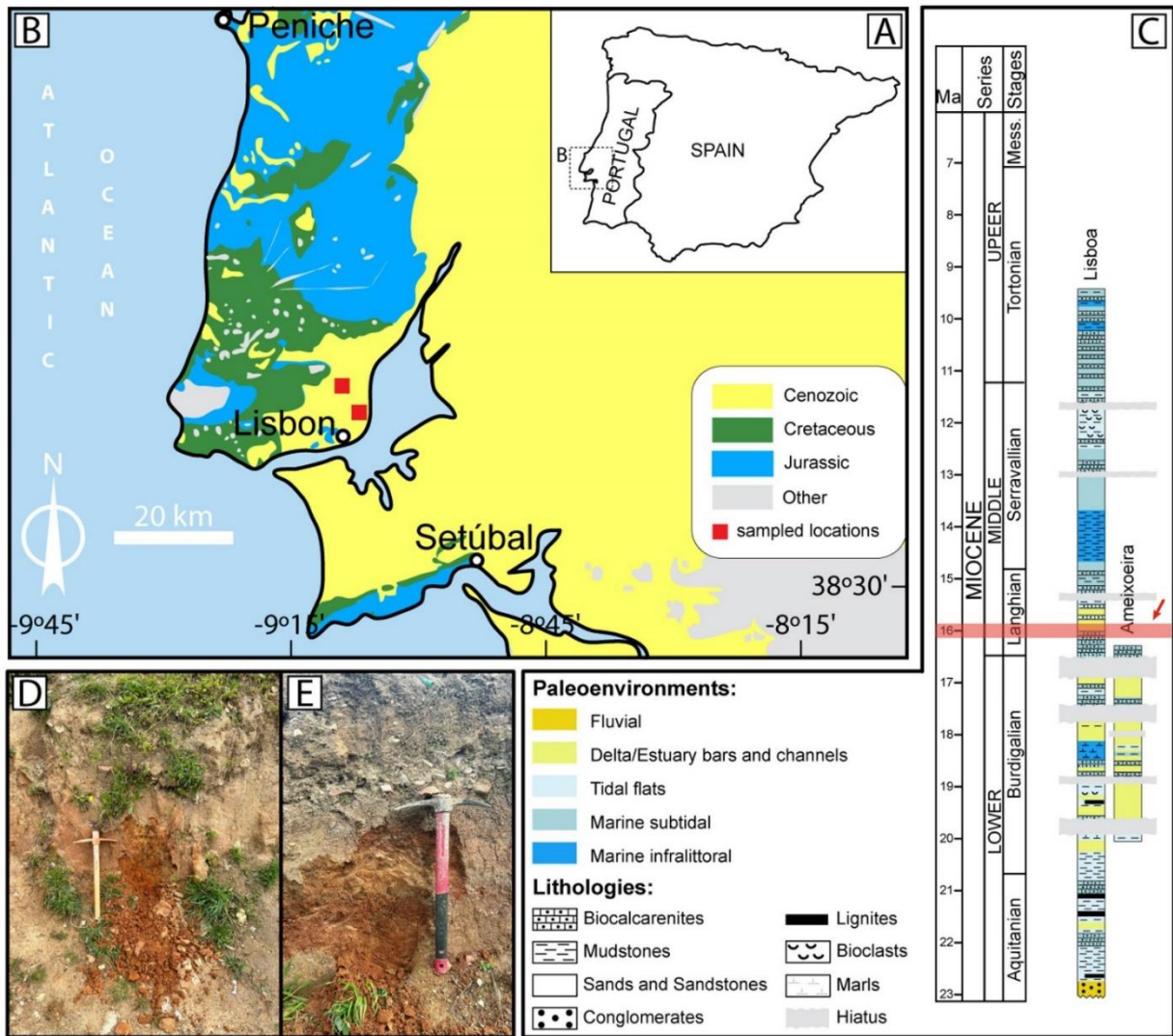
766

767

768

769

770



772

773 **Figure 2.** Geographical setting of the studied areas. A) Location of the Portuguese mainland in the
 774 Iberia Peninsula. B) Regional distribution of main geological outcrops at the Lisbon area (adapted from
 775 LNEG-LGM, 2010). Squares indicate the location of studied sections. C) General biostratigraphic
 776 scheme for the Miocene and stratigraphic context of studied deposits at the Lisbon area (adapted from
 777 Pais et al., 2012). D and E) Field aspect at the localities where the samples were extracted. The molars
 778 analysed in this study originate from the Quinta da Farinheira in the Lower Tagus Basin (Areias do Vale
 779 de Chelas, Lisbon). The Chelas unit has been designated SDL1 by Antunes & Ginsburg (2003) and Vb by
 780 Cotter (1956), with an estimated age of (~15.9–16.1 Ma) and is highlighted by a red arrow. It belongs
 781 to the Langhian stage and the MN5 biozone (13.7–16.0 Ma).

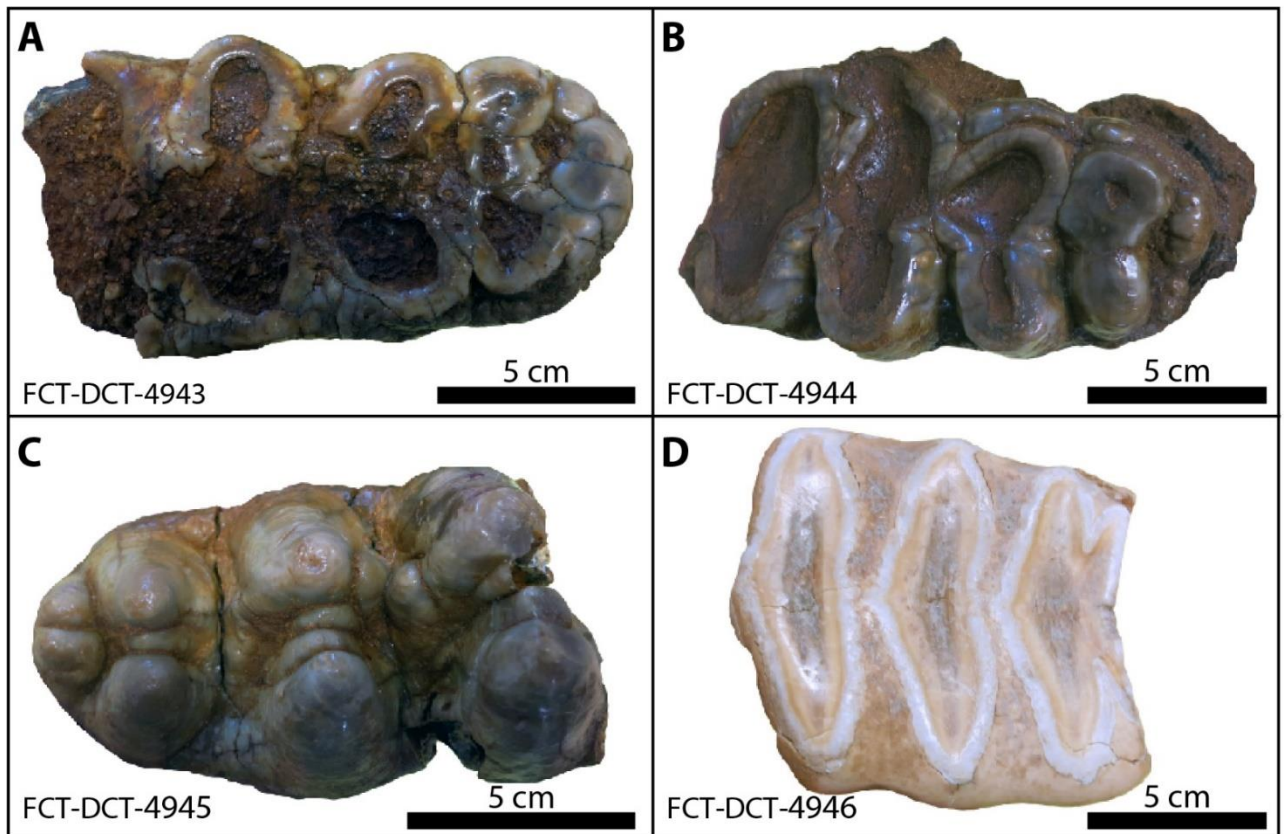
782

783

784

785

786



788

789 **Figure 3.** General aspect of uncut molar samples. A to C) *Gomphotherium angustidens* molars, note
790 less significant wear of the collected samples from A to C. D) Modern *L. Africana* molar, showing typical
791 diamond-shaped ridges.

792

793

794

795

796

797

798

799

800

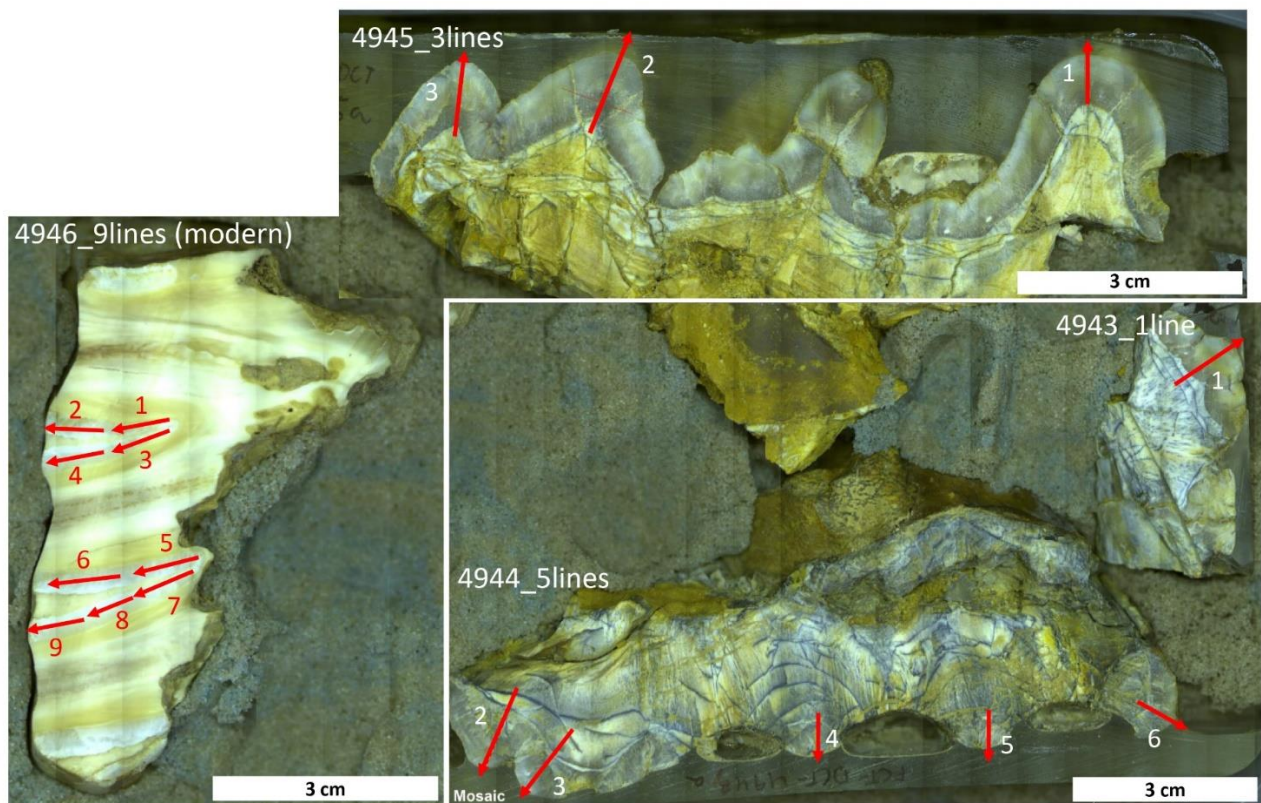
801

802

803

804

805 **Figure 4_Coimbra et al.**



806

807 **Figure 4.** Microscope composite of longitudinally cut modern and Mid-Miocene molar samples with
808 indication of elemental transects chosen for each section (red arrows). Note the inwards-outwards
809 direction of all transects, along growth direction Specimen FCT-DCT 4945 in the top right, FCT-DCT
810 4933 bottom center and FCT-DCT 4943 on the far right. The modern elephant molar is depicted in the
811 bottom left.

812

813

814

815

816

817

818

819

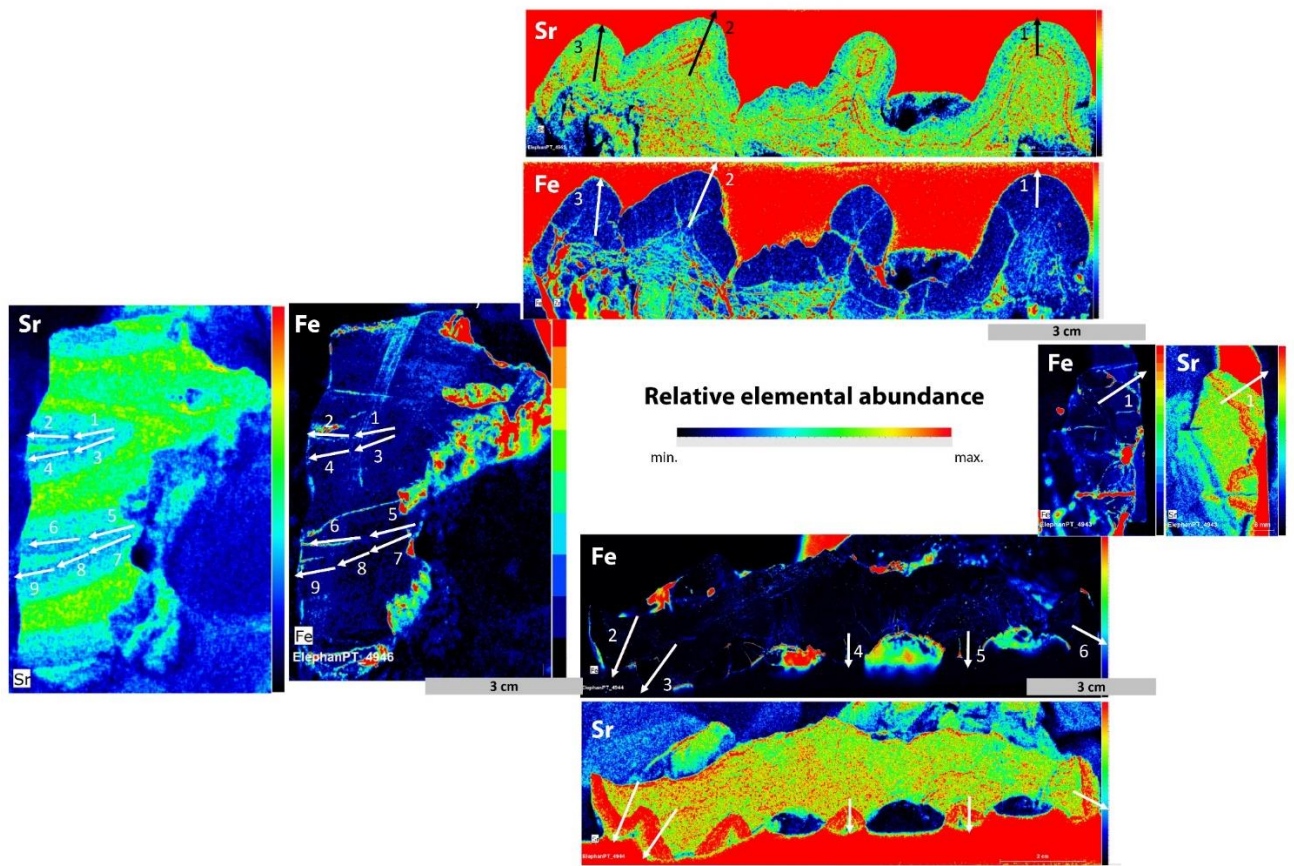
820

821

822

823

824



826

827 **Figure 5.** Relative elemental abundance for all specimen, here shown for iron and strontium
828 (distribution of other elements can be found at <https://doi.org/10.5281/zenodo.14882824>). Note the
829 lack of areas denoting higher iron abundance along selected transects and the clear Sr concentration
830 pattern highlighting well-preserved tooth morphology.

831

832

833

834

835

836

837

838

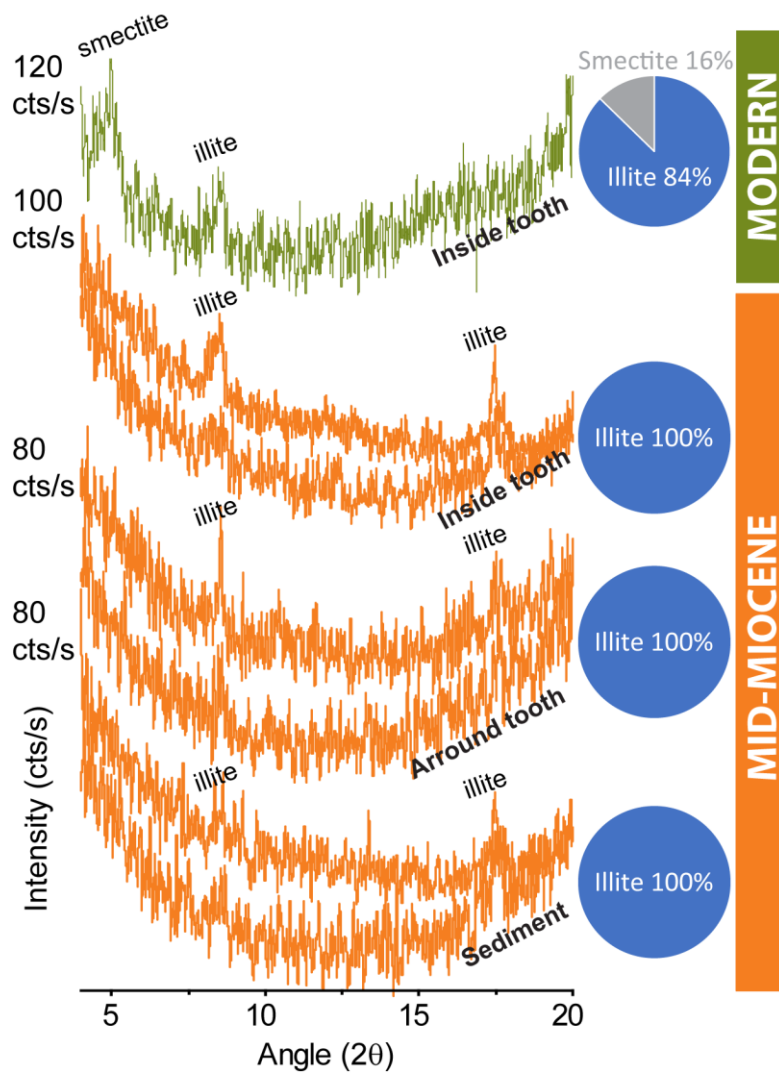
839

840

841

842

843 **Figure 6_Coimbra et al.**



844

845 **Figure 6.** Clay mineral assemblage for Mid-Miocene sediment samples collected from areas adjacent
846 to the molars, around and inside cavities. Modern sediment sample reflects soil substrate from the
847 Lisbon Zoo (see text for details). Note the dominance of illite in all cases, along with minor contribution
848 of smectite for the modern sample.

849

850

851

852

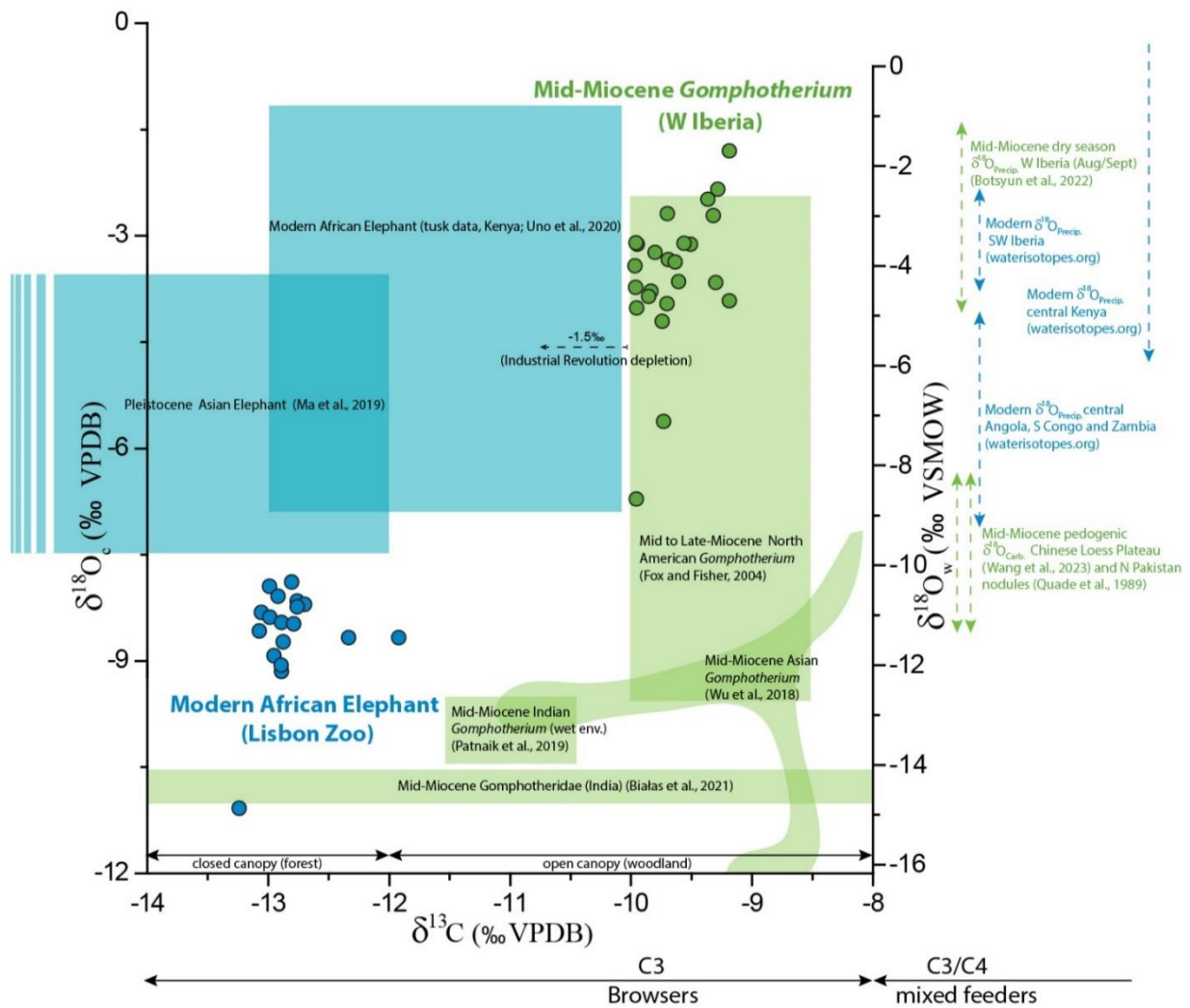
853

854

855

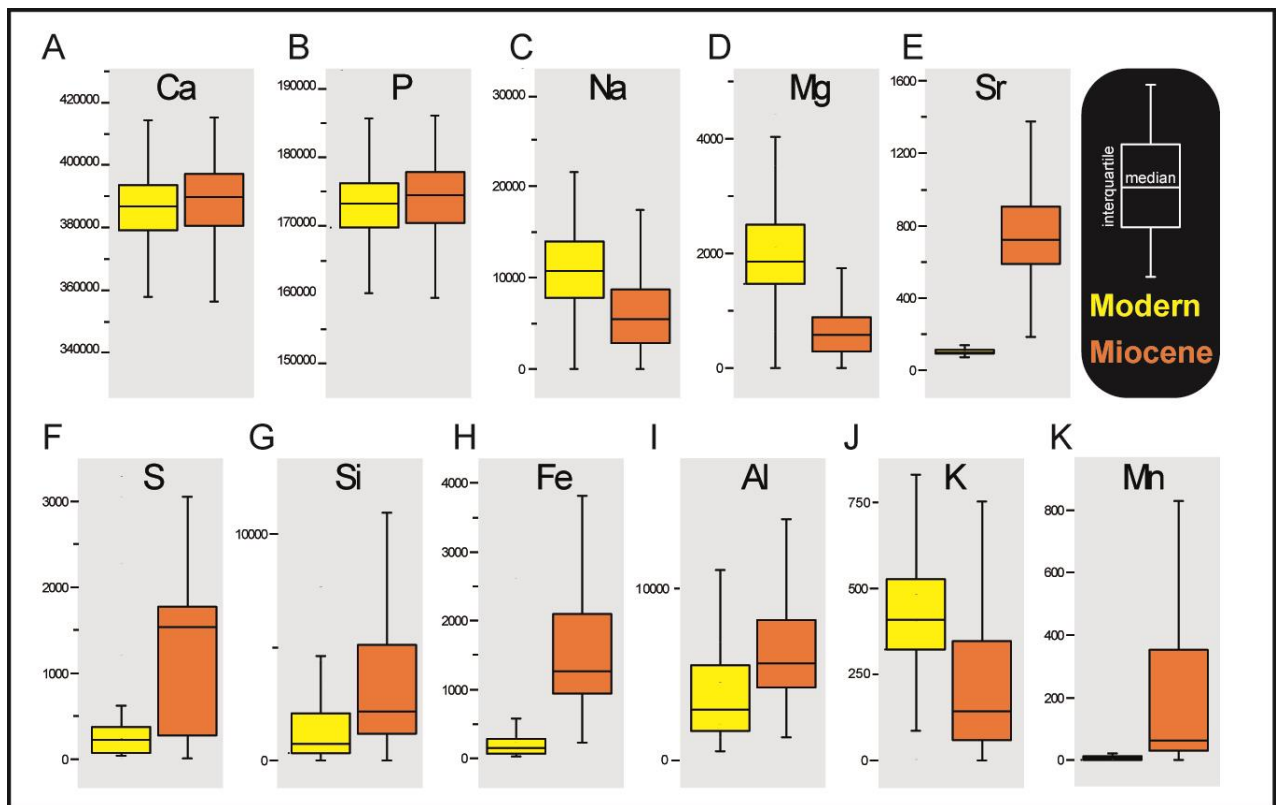
856

857



859
 860 **Figure 7.** Biplot representation of stable carbon and oxygen isotope values, highlighting the differences
 861 between the two sets of samples tested (modern vs. Mid-Miocene). Shaded fields represent C and O
 862 isotope values in enamel-bound carbonate reported by other authors (see reference list) for Mid-
 863 Miocene and modern settings. Vertical arrows indicate range of variation of oxygen isotope values
 864 representative of rainfall composition at different localities (modern and ancient). Oxygen isotope
 865 values of water (right vertical scale) are compared to oxygen isotope values in bioapatite using the
 866 formula for large, water-dependent herbivores from (Hoppe, 2006) and we aligned the VSMOW to
 867 VPDB scale using the formula in (Coplen et al., 1983) following the methodology in (de Rooij et al.,
 868 2022) and (Wooller et al., 2021). Forest/woodlands range of carbon-isotope variation after Patnaik et
 869 al. (2019) and references therein.

870
 871
 872
 873
 874
 875



877

878

879 **Figure 8.** Boxplot representation (median and interquartile distance) of absolute elemental
 880 concentrations (in ppm). A and B) note similar distribution of Ca and P; C and D) lowered values for
 881 ancient samples regarding Na and Mg; E to K) overall higher median values for the remaining proxies
 882 (except K). See Table 2 for full elemental range, mean and standard deviation.

883

884

885

886

887

888

889

890

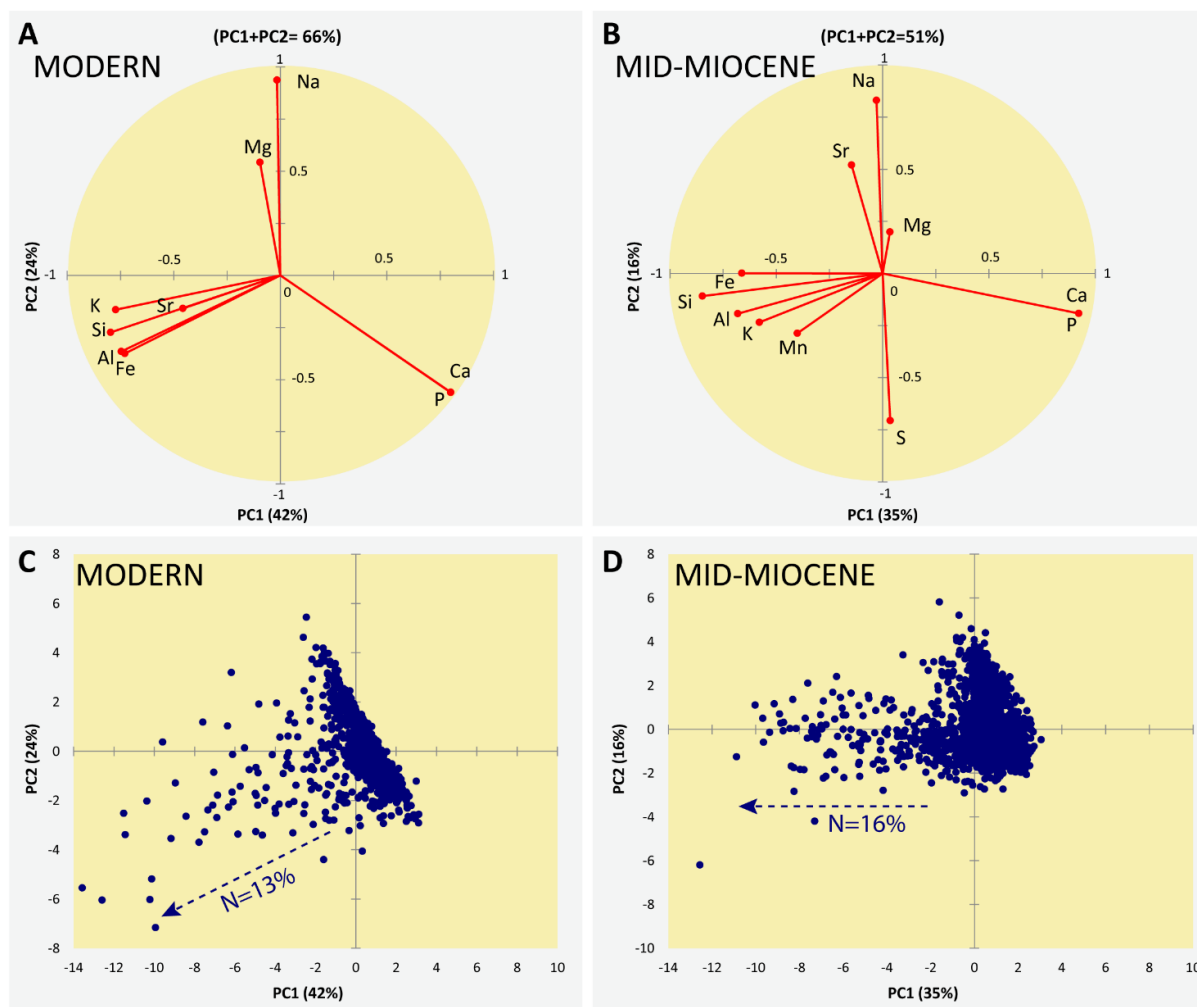
891

892

893

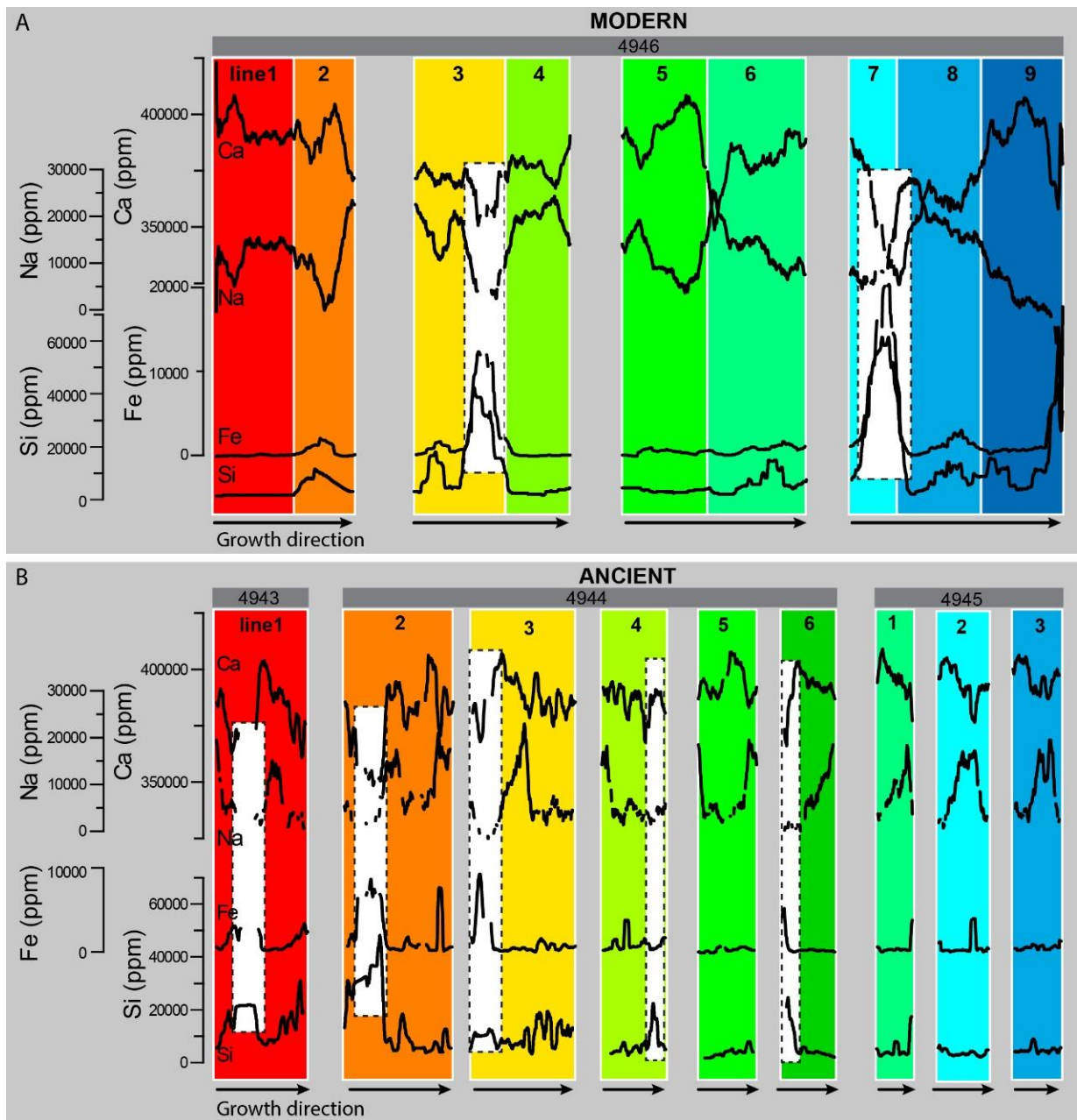
894

895



897
 898 **Figure 9.** Principal component analysis computed for the modern and Mid-Miocene samples. A and B)
 899 Principal component loadings explaining 51 to 66% of the total variability of each set of samples. Note
 900 similar distribution of elements along the PC axis. Modern Mn and S were not used due to low number
 901 of measurements available ($N < 30\%$). C and D) Principal component scores indicating sample
 902 distribution along the PCA space. Note main clusters of samples in both cases, with only few samples
 903 (13% to 16% of the total number of samples) departing from the observed main trend.

904
 905
 906
 907
 908
 909
 910
 911
 912



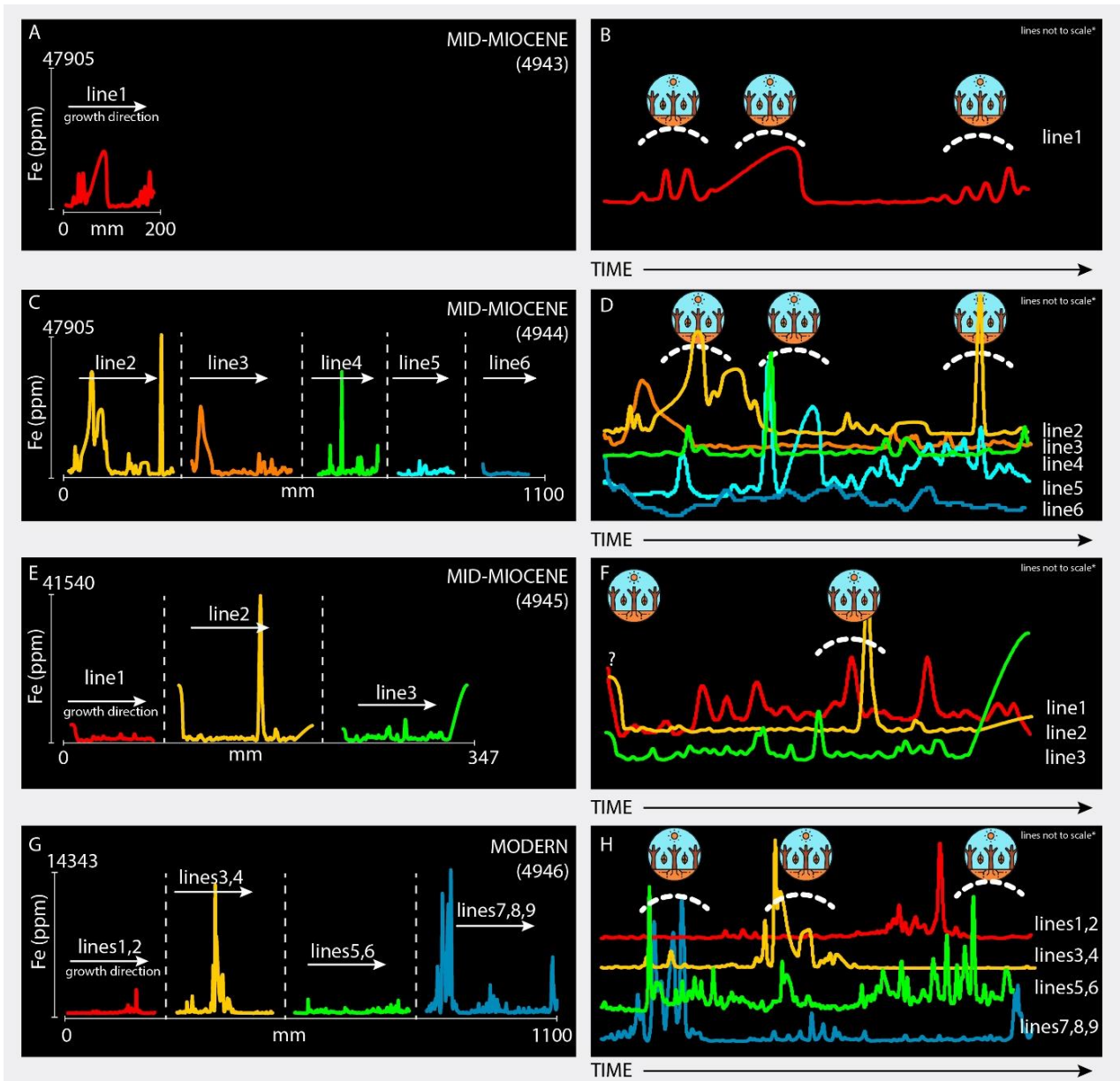
914

915 **Figure 10.** Elemental trend of selected proxies (Ca, Na, Fe and Si) for all measured transects (see Figs.
 916 4 and 5 for exact measurement sites). A) Trend lines for modern transects. B) Trend lines for Mid-
 917 Miocene transects. Note overall similar records of Ca vs. Na and Fe vs. Si, as well as lack of clear
 918 enrichment or depletion trends along each transect. Note opposite variation pattern for Ca and Na,
 919 except when Fe and Si become significantly higher (white dashed boxes). Trend lines smoothed (10
 920 points adjacent averaging); numerals according to Figure 4. Colors represent the different enamel
 921 transects analyzed. The same color scheme is used consistently across all figures to maintain clarity and
 922 allow for easy comparison of the different lines or transects.

923

924

925



927

928 **Figure 11.** Elemental trend line obtained for Fe measurements (line numbers as in Figure 4). A, C E and
 929 G) Record of Fe abundance along growth direction (in mm). B, D F and H) Same datasets stacked and
 930 slightly adjusted (vertically and horizontally) to compare different transects that represent similar
 931 portions of the molar. (*) lines not to scale: mean horizontal scaling factor of 5.1; mean vertical scaling
 932 factor of 3.3 (see Table S1 in Appendix). Drawing represents dry season periods. Colors represent the
 933 different enamel transects analyzed. The same color scheme is used consistently across all figures to
 934 maintain clarity and allow for easy comparison of the different lines or transects.

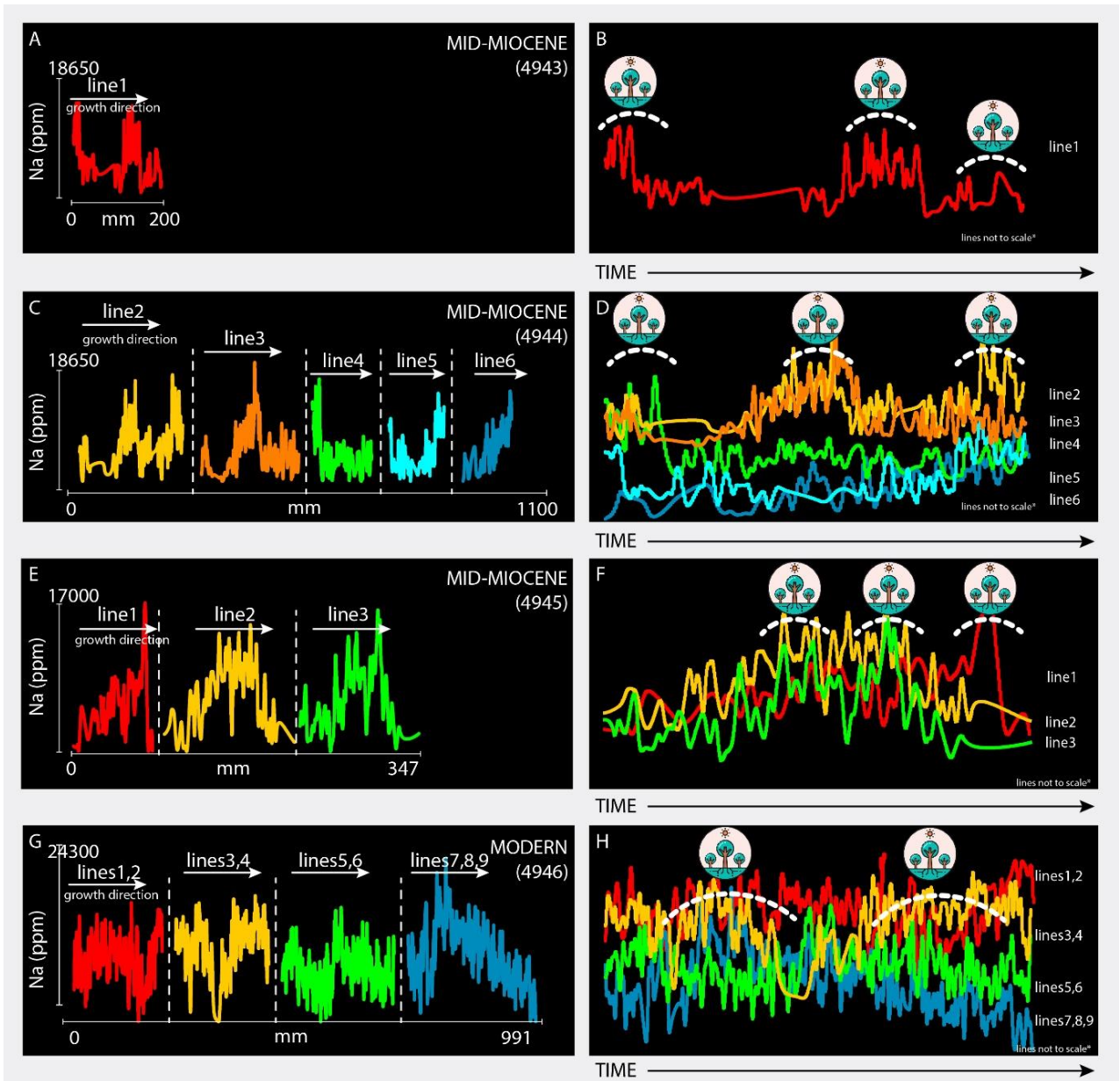
935

936

937

938

939



941

942 **Figure 12.** Elemental trend line obtained for Na measurements (line numbers as in Figure 3). A, C and
 943 E) Record of Na abundance along growth direction (in mm). B, D and F) Same datasets stacked and
 944 slightly adjusted (vertically and horizontally) to compare different transects that represent similar
 945 portions of the molar. (*) lines not to scale: mean horizontal scaling factor of 5.1; mean vertical scaling
 946 factor of 1 (see Table S1 in Appendix). Drawing symbol represents wet season periods. Colors represent
 947 the different enamel transects analyzed. The same color scheme is used consistently across all figures
 948 to maintain clarity and allow for easy comparison of the different lines or transects.

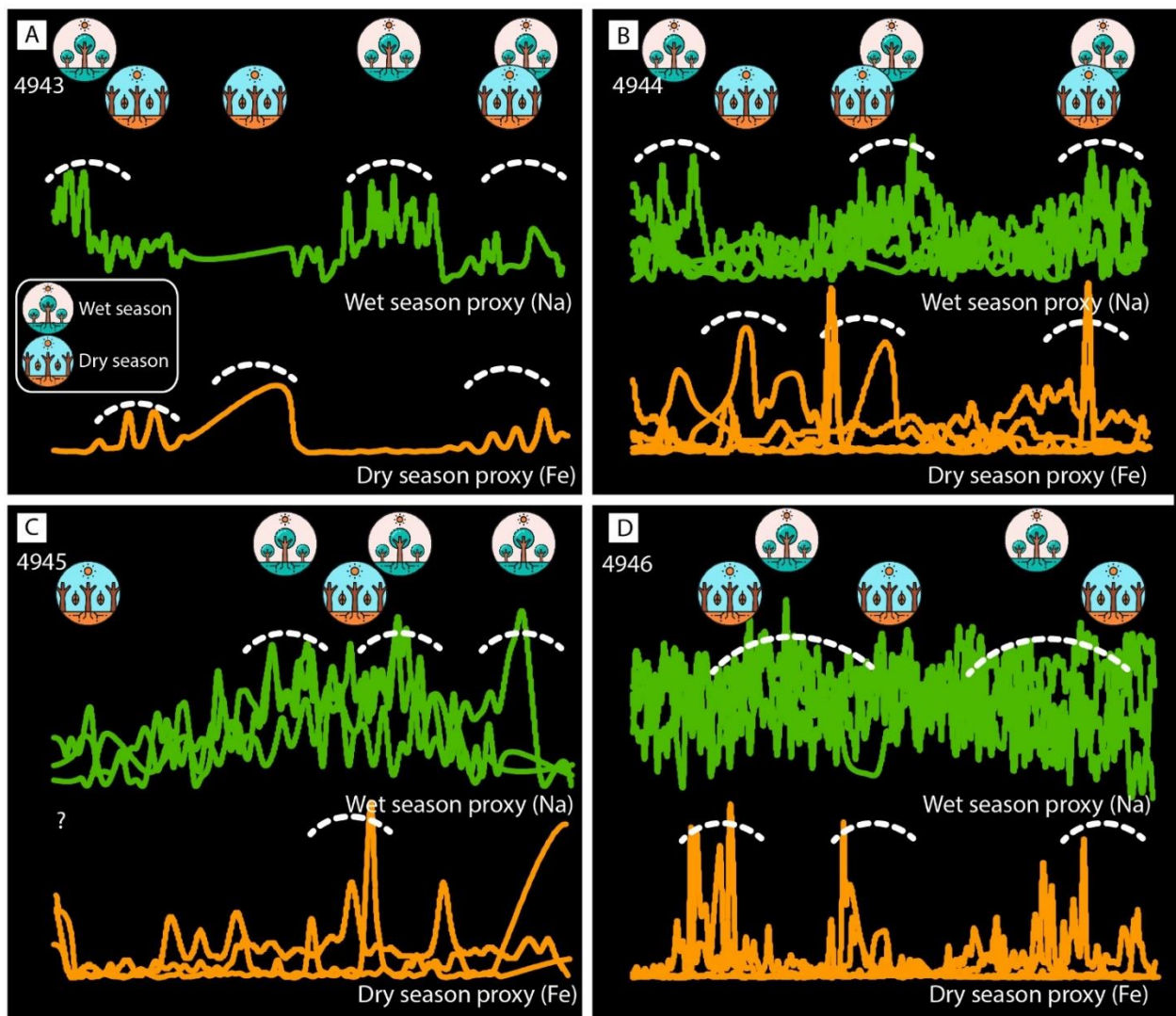
949

950

951

952

953



955
 956 **Figure 13.** Compilation of elemental trend lines for Fe and Na as shown in Figures 11 and 12. A to C)
 957 Mid-Miocene transects in growth direction showing alternating peaks of higher abundance of the
 958 chosen elements. D) Modern transects in growth direction showing alternating peaks of higher
 959 abundance of the chosen elements.

960
 961
 962
 963
 964
 965
 966
 967
 968

969
970
971

Table 1. Semiquantitative abundance (%) of bulk mineralogical composition of sediment samples.

	Quartz	Calcite	Goethite	Ilmenite	Siderite	Dolomite	Observations
Sediment	96	1	3				yellow sediment
	94	2	4				hard crust
Arround Tooth	21		59	20			yellow sediment
	32		41			27	crust
Inside Tooth			100				red hard crust
	67		26		7		yellow sediment
Zoo	52	48					

972
973

Table 2. Mean (\pm standard deviation; s.d.), minimum and maximum elemental values obtained for selected proxies obtained from Miocene and modern samples.

Proxy	Mean	s.d.	min.	Max.	Proxy	Mean	s.d.	min.	Max.	Proxy	Mean	s.d.	min.	Max.
Ca	387428	14136	331284	415258	Na	6042	3982	8	22222	Si	4450	5944	3	44398
	385614	12089	331324	415589		10850	4459	2	26115		3278	7492	2	59156
P	173518	6331	148372	185982	Mg	645	465	1	4435	Fe	2621	4657	225	56135
	172706	5414	148391	186130		2383	1831	2	15502		428	1357	26	18381
MIOCENE MODERN					Sr	755	224	185	1510	Al	6891	4017	1332	25596
						107	34	63	722		4547	4825	512	45641
					S	1215	755	1	3046	K	403	701	0	5636
				246		164	40	617	485		342	85	4276	
										Mn	506	1391	0	26942
											18	48	0	365

974
975
976
977
978
979
980
981
982

983 **References**

- 984 Abrahams, P.W., Parsons, J.A., 1996. Geophagy in the Tropics: A Literature Review. *The Geographical*
 985 *Journal* 162, 63–72. <https://doi.org/10.2307/3060216>
- 986 Antunes, M.T., Ginsburg, L., 2003. The last Anthracothere *Brachyodus onoideus* (Mammalia,
 987 *Artiodactyla*) from westernmost Europe and its extinction. *Ciências da Terra* 15, 161–172.
- 988 Antunes, M.T., Pais, J., 1984. Climate during Miocene in Portugal and its evolution. *Paléobiologie*
 989 *continentale* 14, 75–89.
- 990 Aoba, T., Moreno, E.C., Shimoda, S., 1992a. Competitive adsorption of magnesium and calcium ions
 991 onto synthetic and biological apatites. *Calcif Tissue Int* 51, 143–150.
 992 <https://doi.org/10.1007/BF00298503>
- 993 Aoba, T., Shimoda, S., Moreno, E.C., 1992b. Labile or surface pools of magnesium, sodium, and
 994 potassium in developing porcine enamel mineral. *J Dent Res* 71, 1826–1831.
 995 <https://doi.org/10.1177/00220345920710111201>
- 996 Ayliffe, L.K., Chivas, A.R., 1990. Oxygen isotope composition of the bone phosphate of Australian
 997 kangaroos: Potential as a palaeoenvironmental recorder. *Geochimica et Cosmochimica Acta*
 998 54, 2603–2609. [https://doi.org/10.1016/0016-7037\(90\)90246-H](https://doi.org/10.1016/0016-7037(90)90246-H)
- 999 Ayliffe, L.K., Lister, A.M., Chivas, A.R., 1992. The preservation of glacial-interglacial climatic signatures
 1000 in the oxygen isotopes of elephant skeletal phosphate. *Palaeogeography, Palaeoclimatology,*
 1001 *Palaeoecology* 99, 179–191. [https://doi.org/10.1016/0031-0182\(92\)90014-V](https://doi.org/10.1016/0031-0182(92)90014-V)
- 1002 Beauvais, A., Colin, F., 1993. Formation and transformation processes of iron duricrust systems in
 1003 tropical humid environment. *Chemical Geology* 106, 77–101. [https://doi.org/10.1016/0009-2541\(93\)90167-H](https://doi.org/10.1016/0009-2541(93)90167-H)
- 1004
- 1005 Bender, M.M., 1971. Variations in the $^{13}\text{C}/^{12}\text{C}$ ratios of plants in relation to the pathway of
 1006 photosynthetic carbon dioxide fixation. *Phytochemistry* 10, 1239–1244.
 1007 [https://doi.org/10.1016/S0031-9422\(00\)84324-1](https://doi.org/10.1016/S0031-9422(00)84324-1)
- 1008 Bhavya, S., 2017. 3 Main Types of Teeth Found in Mammals | Vertebrates | Chordata | Zoology.
 1009 *Zoology Notes*. URL [https://www.notesonzooology.com/mammals/3-main-types-of-teeth-](https://www.notesonzooology.com/mammals/3-main-types-of-teeth-found-in-mammals-vertebrates-chordata-zoology/8495)
 1010 [found-in-mammals-vertebrates-chordata-zoology/8495](https://www.notesonzooology.com/mammals/3-main-types-of-teeth-found-in-mammals-vertebrates-chordata-zoology/8495) (accessed 1.10.24).
- 1011 Białaś, N., Prymak, O., Singh, N.P., Paul, D., Patnaik, R., Epple, M., 2021. Teeth of Past and Present
 1012 Elephants: Microstructure and Composition of Enamel in Fossilized Proboscidean Molars and
 1013 Implications for Diagenesis. *Geochemistry, Geophysics, Geosystems* 22, e2020GC009557.
 1014 <https://doi.org/10.1029/2020GC009557>
- 1015 Blaise, E., Balasse, M., 2011. Seasonality and season of birth of modern and late Neolithic sheep from
 1016 south-eastern France using tooth enamel $\delta^{18}\text{O}$ analysis. *Journal of archaeological Science*
 1017 38, 3085–3093.
- 1018 Botsyun, S., Ehlers, T.A., Koptev, A., Böhme, M., Methner, K., Risi, C., Stepanek, C., Mutz, S.G., Werner,
 1019 M., Boateng, D., Mulch, A., 2022. Middle Miocene Climate and Stable Oxygen Isotopes in
 1020 Europe Based on Numerical Modeling. *Paleoceanography and Paleoclimatology* 37,
 1021 e2022PA004442. <https://doi.org/10.1029/2022PA004442>
- 1022 Brown, G., Brindley, G.W., 1980. X-ray Diffraction Procedures for Clay Mineral Identification, in:
 1023 Brindley, G.W., Brown, G. (Eds.), *Crystal Structures of Clay Minerals and Their X-Ray*
 1024 *Identification*. Mineralogical Society of Great Britain and Ireland, p. 0.
 1025 <https://doi.org/10.1180/mono-5.5>
- 1026 Brüggmann, G., Krause, J., Brachert, T.C., Stoll, B., Weis, U., Kullmer, O., Ssemmanda, I., Mertz, D.F.,
 1027 2012. Chemical composition of modern and fossil hippopotamid teeth and implications for
 1028 paleoenvironmental reconstructions and enamel formation – Part 2: Alkaline earth
 1029 elements as tracers of watershed hydrochemistry and provenance. *Biogeosciences* 9, 4803–
 1030 4817. <https://doi.org/10.5194/bg-9-4803-2012>
- 1031 Bryant, J.D., Froelich, P.N., Showers, W.J., Genna, B.J., 1996. Biologic and climatic signals in the oxygen
 1032 isotopic composition of Eocene-Oligocene equid enamel phosphate. *Palaeogeography,*

1033 Palaeoclimatology, Palaeoecology, Biogenic Phosphates as Palaeoenvironmental Indicators
1034 126, 75–89. [https://doi.org/10.1016/S0031-0182\(96\)00071-5](https://doi.org/10.1016/S0031-0182(96)00071-5)

1035 Burls, N.J., Bradshaw, C.D., De Boer, A.M., Herold, N., Huber, M., Pound, M., Donnadieu, Y.,
1036 Farnsworth, A., Frigola, A., Gasson, E., von der Heydt, A.S., Hutchinson, D.K., Knorr, G.,
1037 Lawrence, K.T., Lear, C.H., Li, X., Lohmann, G., Lunt, D.J., Marzocchi, A., Prange, M., Riihimaki,
1038 C.A., Sarr, A.-C., Siler, N., Zhang, Z., 2021. Simulating Miocene Warmth: Insights From an
1039 Opportunistic Multi-Model Ensemble (MioMIP1). *Paleoceanography and Paleoclimatology*
1040 36, e2020PA004054. <https://doi.org/10.1029/2020PA004054>

1041 Cantalapiedra, J.L., Sanisidro, Ó., Zhang, H., Alberdi, M.T., Prado, J.L., Blanco, F., Saarinen, J., 2021. The
1042 rise and fall of proboscidean ecological diversity. *Nat Ecol Evol* 5, 1266–1272.
1043 <https://doi.org/10.1038/s41559-021-01498-w>

1044 Cerling, T.E., Harris, J.M., 1999. Carbon isotope fractionation between diet and bioapatite in ungulate
1045 mammals and implications for ecological and paleoecological studies. *Oecologia* 120, 347–
1046 363.

1047 Cerling, T.E., Harris, J.M., Ambrose, S.H., Leakey, M.G., Solounias, N., 1997a. Dietary and
1048 environmental reconstruction with stable isotope analyses of herbivore tooth enamel from
1049 the Miocene locality of Fort Ternan, Kenya. *Journal of Human Evolution* 33, 635–650.

1050 Cerling, T.E., Harris, J.M., Leakey, M.G., 2003a. 12.2. Isotope Paleocology of the Nawata and
1051 Nachukui Formations at Lothagam, Turkana Basin, Kenya, in: 12.2. Isotope Paleocology of
1052 the Nawata and Nachukui Formations at Lothagam, Turkana Basin, Kenya. Columbia
1053 University Press, pp. 605–624. <https://doi.org/10.7312/leak11870-024>

1054 Cerling, T.E., Harris, J.M., Leakey, M.G., Mudida, N., 2003b. 12.1. Stable Isotope Ecology of Northern
1055 Kenya, with Emphasis on the Turkana Basin, in: 12.1. Stable Isotope Ecology of Northern
1056 Kenya, with Emphasis on the Turkana Basin. Columbia University Press, pp. 583–604.
1057 <https://doi.org/10.7312/leak11870-023>

1058 Cerling, T.E., Harris, J.M., MacFadden, B.J., Leakey, M.G., Quade, J., Eisenmann, V., Ehleringer, J.R.,
1059 1997b. Global vegetation change through the Miocene/Pliocene boundary. *Nature* 389, 153.

1060 Cerling, T.E., Hart, J.A., Hart, T.B., 2004. Stable isotope ecology in the Ituri Forest. *Oecologia* 138, 5–
1061 12. <https://doi.org/10.1007/s00442-003-1375-4>

1062 Chandrajith, R., Kudavidanage, E., Tobschall, H.J., Dissanayake, C.B., 2009. Geochemical and
1063 mineralogical characteristics of elephant geophagic soils in Udawalawe National Park, Sri
1064 Lanka. *Environ Geochem Health* 31, 391–400. <https://doi.org/10.1007/s10653-008-9178-5>

1065 Clementz, M.T., 2012. New insight from old bones: stable isotope analysis of fossil mammals. *Journal*
1066 *of Mammalogy* 93, 368–380. <https://doi.org/10.1644/11-MAMM-S-179.1>

1067 Coimbra, R., Huck, S., de Winter, N.J., Heimhofer, U., Claeys, P., 2020. Improving the detection of shell
1068 alteration: Implications for sclerochronology. *Palaeogeography, Palaeoclimatology,*
1069 *Palaeoecology* 559, 109968. <https://doi.org/10.1016/j.palaeo.2020.109968>

1070 Coplen, T.B., Kendall, C., Hopple, J., 1983. Comparison of stable isotope reference samples. *Nature*
1071 302, 236–238. <https://doi.org/10.1038/302236a0>

1072 de Rooij, J., van der Lubbe, J.H.J.L., Verdegaal, S., Hulscher, M., Tooms, D., Kaskes, P., Verhage, O.,
1073 Portanger, L., Schulp, A.S., 2022. Stable isotope record of *Triceratops* from a mass
1074 accumulation (Lance Formation, Wyoming, USA) provides insights into *Triceratops* behaviour
1075 and ecology. *Palaeogeography, Palaeoclimatology, Palaeoecology* 607, 111274.
1076 <https://doi.org/10.1016/j.palaeo.2022.111274>

1077 de Winter, N., Sinnesael, M., Makarona, C., Vansteenberge, S., Claeys, P., 2017. Trace element
1078 analyses of carbonates using portable and micro-X-ray fluorescence: Performance and
1079 optimization of measurement parameters and strategies. *Journal of Analytical Atomic*
1080 *Spectrometry*. <https://doi.org/10.1039/c6ja00361c>

1081 De Winter, N., Snoeck, C., Claeys, P., 2016. Seasonal cyclicity in trace elements and stable isotopes of
1082 modern horse enamel. *PLoS ONE* 11, 1. <https://doi.org/10.1371/journal.pone.0166678>

1083 de Winter, N.J., Claeys, P., 2016. Micro X-ray fluorescence (μ XRF) line scanning on Cretaceous rudist
1084 bivalves: A new method for reproducible trace element profiles in bivalve calcite.
1085 *Sedimentology* 64, 231–251. <https://doi.org/10.1111/sed.12299>
1086 de Winter, N.J., Snoeck, C., Schulting, R., Fernández-Crespo, T., Claeys, P., 2019. High-resolution trace
1087 element distributions and models of trace element diffusion in enamel of Late Neolithic/Early
1088 Chalcolithic human molars from the Rioja Alavesa region (north-central Spain) help to
1089 separate biogenic from diagenetic trends. *Palaeogeography, Palaeoclimatology,*
1090 *Palaeoecology* 532, 109260. <https://doi.org/10.1016/j.palaeo.2019.109260>
1091 Díaz-Hernández, J.L., Sánchez-Navas, A., Reyes, E., 2013. Isotopic evidence for dolomite formation in
1092 soils. *Chemical Geology* 347, 20–33. <https://doi.org/10.1016/j.chemgeo.2013.03.018>
1093 Dirks, W., Bromage, T.G., Agenbroad, L.D., 2012. The duration and rate of molar plate formation in
1094 *Palaeoloxodon cypristes* and *Mammuthus columbi* from dental histology. *Quaternary*
1095 *International, Mammoths and Their Relatives 1: Biotopes, Evolution and Human Impact V*
1096 *International Conference, Le Puy-en-Velay, 2010* 255, 79–85.
1097 <https://doi.org/10.1016/j.quaint.2011.11.002>
1098 Domingo, L., Cuevas-González, J., Grimes, S.T., Fernández, M.H., López-Martínez, N., 2009. Multiproxy
1099 reconstruction of the palaeoclimate and palaeoenvironment of the Middle Miocene
1100 Somosaguas site (Madrid, Spain) using herbivore dental enamel. *Palaeogeography,*
1101 *Palaeoclimatology, Palaeoecology* 272, 53–68.
1102 Ehleringer, J.R., Sage, R.F., Flanagan, L.B., Pearcy, R.W., 1991. Climate change and the evolution of C4
1103 photosynthesis. *Trends in Ecology & Evolution* 6, 95–99. [https://doi.org/10.1016/0169-](https://doi.org/10.1016/0169-5347(91)90183-X)
1104 [5347\(91\)90183-X](https://doi.org/10.1016/0169-5347(91)90183-X)
1105 Esker, D., Forman, S.L., Widga, C., Walker, J.D., Andrew, J.E., 2019. Home range of the Columbian
1106 mammoths (*Mammuthus columbi*) and grazing herbivores from the Waco Mammoth
1107 National Monument, (Texas, USA) based on strontium isotope ratios from tooth enamel
1108 bioapatite. *Palaeogeography, Palaeoclimatology, Palaeoecology* 534, 109291.
1109 <https://doi.org/10.1016/j.palaeo.2019.109291>
1110 Farquhar, G.D., Ehleringer, J.R., Hubick, K.T., 1989. Carbon isotope discrimination and photosynthesis.
1111 *Annual review of plant biology* 40, 503–537.
1112 Forbes, M.S., Kohn, M.J., Bestland, E.A., Wells, R.T., 2010. Late Pleistocene environmental change
1113 interpreted from $\delta^{13}\text{C}$ and $\delta^{18}\text{O}$ of tooth enamel from the Black Creek Swamp Megafauna
1114 site, Kangaroo Island, South Australia. *Palaeogeography, Palaeoclimatology, Palaeoecology*
1115 291, 319–327. <https://doi.org/10.1016/j.palaeo.2010.03.003>
1116 Fox, D.L., Fisher, D.C., 2004. Dietary reconstruction of Miocene Gomphotherium (Mammalia,
1117 Proboscidea) from the Great Plains region, USA, based on the carbon isotope composition of
1118 tusk and molar enamel. *Palaeogeography, Palaeoclimatology, Palaeoecology, Incremental*
1119 *Growth in Vertebrate Skeletal Tissues: Paleobiological and Paleoenvironmental Implications*
1120 206, 311–335. <https://doi.org/10.1016/j.palaeo.2004.01.010>
1121 Fricke, H.C., O’Neil, J.R., 1996. Inter- and intra-tooth variation in the oxygen isotope composition of
1122 mammalian tooth enamel phosphate: implications for palaeoclimatological and
1123 palaeobiological research. *Palaeogeography, Palaeoclimatology, Palaeoecology, Biogenic*
1124 *Phosphates as Palaeoenvironmental Indicators* 126, 91–99. [https://doi.org/10.1016/S0031-](https://doi.org/10.1016/S0031-0182(96)00072-7)
1125 [0182\(96\)00072-7](https://doi.org/10.1016/S0031-0182(96)00072-7)
1126 Galhano, C., Rocha, F., Gomes, C., 1999. Geostatistical analysis of the influence of textural,
1127 mineralogical and geochemical parameters on the geotechnical behaviour of the ‘Argilas de
1128 Aveiro’ Formation (Portugal). *Clay Minerals* 34, 109–116.
1129 <https://doi.org/10.1180/000985599545966>
1130 Geraads, D., Zouhri, S., Markov, G.N., 2019. The first Tetralophodon (Mammalia, Proboscidea)
1131 cranium from Africa. *Journal of Vertebrate Paleontology* 39, e1632321.
1132 <https://doi.org/10.1080/02724634.2019.1632321>

1133 Gill, J.L., Williams, J.W., Jackson, S.T., Lininger, K.B., Robinson, G.S., 2009. Pleistocene Megafaunal
1134 Collapse, Novel Plant Communities, and Enhanced Fire Regimes in North America. *Science*
1135 326, 1100–1103. <https://doi.org/10.1126/science.1179504>
1136 Goldner, A., Herold, N., Huber, M., 2014. The challenge of simulating the warmth of the mid-Miocene
1137 climatic optimum in CESM1. *Climate of the Past* 10, 523–536. [https://doi.org/10.5194/cp-10-](https://doi.org/10.5194/cp-10-523-2014)
1138 523-2014
1139 Gomphotherium angustidens by cisiopurple on DeviantArt [WWW Document], 2022. URL
1140 <https://www.deviantart.com/cisiopurple/art/Gomphotherium-angustidens-916106115>
1141 (accessed 1.10.24).
1142 Harzhauser, M., Kroh, A., Mandic, O., Piller, W.E., Göhlich, U., Reuter, M., Berning, B., 2007.
1143 Biogeographic responses to geodynamics: A key study all around the Oligo–Miocene Tethyan
1144 Seaway. *Zoologischer Anzeiger - A Journal of Comparative Zoology, Special Issue: Phylogenetic*
1145 *Symposium* 246, 241–256. <https://doi.org/10.1016/j.jcz.2007.05.001>
1146 Harzhauser, M., Piller, W.E., Müllegger, S., Grunert, P., Micheels, A., 2011. Changing seasonality
1147 patterns in Central Europe from Miocene Climatic Optimum to Miocene Climate Transition
1148 deduced from the *Crassostrea* isotope archive. *Global and Planetary Change* 76, 77–84.
1149 <https://doi.org/10.1016/j.gloplacha.2010.12.003>
1150 He, Z., Zhang, Z., Guo, Z., Scotese, C.R., Deng, C., 2023. An early Miocene (~20 Ma) paleogeographic
1151 reconstruction for paleoclimate modelling. *Palaeogeography, Palaeoclimatology,*
1152 *Palaeoecology* 612, 111382. <https://doi.org/10.1016/j.palaeo.2022.111382>
1153 Holbourn, A., Kuhnt, W., Kochhann, K.G.D., Andersen, N., Sebastian Meier, K.J., 2015. Global
1154 perturbation of the carbon cycle at the onset of the Miocene Climatic Optimum. *Geology* 43,
1155 123–126. <https://doi.org/10.1130/G36317.1>
1156 Holdø, R.M., Dudley, J.P., McDowell, L.R., 2002. Geophagy in the African Elephant in Relation to
1157 Availability of Dietary Sodium. *Journal of Mammalogy* 83, 652–664.
1158 [https://doi.org/10.1644/1545-1542\(2002\)083%253C0652:GITAEI%253E2.0.CO;2](https://doi.org/10.1644/1545-1542(2002)083%253C0652:GITAEI%253E2.0.CO;2)
1159 Hoppe, K.A., 2006. Correlation between the oxygen isotope ratio of North American bison teeth and
1160 local waters: Implication for paleoclimatic reconstructions. *Earth and Planetary Science*
1161 *Letters* 244, 408–417. <https://doi.org/10.1016/j.epsl.2006.01.062>
1162 Houston, D.C., Gilardi, J.D., Hall, A.J., 2001. Soil consumption by Elephants might help to minimize the
1163 toxic effects of plant secondary compounds in forest browse. *Mammal Review* 31, 249–254.
1164 <https://doi.org/10.1111/j.1365-2907.2001.00091.x>
1165 Iannucci, A., Sardella, R., 2023. What Does the “Elephant-Equus” Event Mean Today? Reflections on
1166 Mammal Dispersal Events around the Pliocene-Pleistocene Boundary and the Flexible
1167 Ambiguity of Biochronology. *Quaternary* 6, 16. <https://doi.org/10.3390/quat6010016>
1168 IPCC, 2023. SYNTHESIS REPORT OF THE IPCC SIXTH ASSESSMENT REPORT (AR6). Intergovernmental
1169 Panel on Climate Change, Geneva, Switzerland.
1170 Ito, A., Wagai, R., 2017. Global distribution of clay-size minerals on land surface for biogeochemical
1171 and climatological studies. *Sci Data* 4, 170103. <https://doi.org/10.1038/sdata.2017.103>
1172 Jayachandran, M., 2022. The Role of Molar Teeth In Age Determination of Elephants [WWW
1173 Document]. *Wildlife SOS*. URL [https://wildlifesos.org/elephant/the-role-of-molar-teeth-in-](https://wildlifesos.org/elephant/the-role-of-molar-teeth-in-age-determination-of-elephants/)
1174 [age-determination-of-elephants/](https://wildlifesos.org/elephant/the-role-of-molar-teeth-in-age-determination-of-elephants/) (accessed 1.10.24).
1175 Journet, E., Balkanski, Y., Harrison, S.P., 2014. A new data set of soil mineralogy for dust-cycle
1176 modeling. *Atmospheric Chemistry and Physics* 14, 3801–3816. [https://doi.org/10.5194/acp-](https://doi.org/10.5194/acp-14-3801-2014)
1177 14-3801-2014
1178 Koch, P.L., Michener, R., Lajtha, K., 2007. Isotopic study of the biology of modern and fossil
1179 vertebrates. *Stable isotopes in ecology and environmental science* 2, 99–154.
1180 Kohn, M.J., 2008. Models of diffusion-limited uptake of trace elements in fossils and rates of
1181 fossilization. *Geochimica et Cosmochimica Acta* 72, 3758–3770.
1182 <https://doi.org/10.1016/j.gca.2008.05.045>

1183 Kohn, M.J., 1996. Predicting animal $\delta^{18}\text{O}$: Accounting for diet and physiological adaptation.
1184 *Geochimica et Cosmochimica Acta* 60, 4811–4829. [https://doi.org/10.1016/S0016-](https://doi.org/10.1016/S0016-7037(96)00240-2)
1185 [7037\(96\)00240-2](https://doi.org/10.1016/S0016-7037(96)00240-2)

1186 Kohn, M.J., Cerling, T.E., 2002. Stable Isotope Compositions of Biological Apatite. *Reviews in*
1187 *Mineralogy and Geochemistry* 48, 455–488. <https://doi.org/10.2138/rmg.2002.48.12>

1188 Kohn, M.J., Morris, J., Olin, P., 2013. Trace element concentrations in teeth – a modern Idaho baseline
1189 with implications for archeometry, forensics, and palaeontology. *Journal of Archaeological*
1190 *Science* 40, 1689–1699. <https://doi.org/10.1016/j.jas.2012.11.012>

1191 Kohn, M.J., Schoeninger, M.J., Barker, W.W., 1999. Altered states: effects of diagenesis on fossil tooth
1192 chemistry. *Geochimica et Cosmochimica Acta* 63, 2737–2747.

1193 Kohn, M.J., Schoeninger, M.J., Valley, J.W., 1996. Herbivore tooth oxygen isotope compositions: Effects
1194 of diet and physiology. *Geochimica et Cosmochimica Acta* 60, 3889–3896.
1195 [https://doi.org/10.1016/0016-7037\(96\)00248-7](https://doi.org/10.1016/0016-7037(96)00248-7)

1196 Kowalik, N., Anczkiewicz, R., Müller, W., Spötl, C., Bondioli, L., Nava, A., Wojtal, P., Wilczyński, J.,
1197 Koziarska, M., Matyszczak, M., 2023. Revealing seasonal woolly mammoth migration with
1198 spatially-resolved trace element, Sr and O isotopic records of molar enamel. *Quaternary*
1199 *Science Reviews* 306, 108036. <https://doi.org/10.1016/j.quascirev.2023.108036>

1200 Kübler, B., Jaboyedoff, M., 2000. Illite crystallinity. *Comptes Rendus de l'Académie des Sciences -*
1201 *Series IIA - Earth and Planetary Science* 331, 75–89. [https://doi.org/10.1016/S1251-](https://doi.org/10.1016/S1251-8050(00)01395-1)
1202 [8050\(00\)01395-1](https://doi.org/10.1016/S1251-8050(00)01395-1)

1203 Larramendi, A., 2015. Shoulder Height, Body Mass, and Shape of Proboscideans. *acpp* 61, 537–574.
1204 <https://doi.org/10.4202/app.00136.2014>

1205 Lee, P.C., Sayialel, S., Lindsay, W.K., Moss, C.J., 2012. African elephant age determination from teeth:
1206 validation from known individuals. *African Journal of Ecology* 50, 9–20.
1207 <https://doi.org/10.1111/j.1365-2028.2011.01286.x>

1208 Lee-Thorp, J., Sponheimer, M., 2003. Three case studies used to reassess the reliability of fossil bone
1209 and enamel isotope signals for paleodietary studies. *Journal of Anthropological Archaeology*
1210 22, 208–216.

1211 LeGeros, R.Z., 1986. Variability of HAP/b-TCP ratios in sintered apatites, in: *Journal of Dental*
1212 *Research*. AMER ASSOC DENTAL RESEARCH 1619 DUKE ST, ALEXANDRIA, VA 22314, pp. 292–
1213 292.

1214 Levin, N.E., Cerling, T.E., Passey, B.H., Harris, J.M., Ehleringer, J.R., 2006. A stable isotope aridity index
1215 for terrestrial environments. *Proceedings of the National Academy of Sciences* 103, 11201–
1216 11205. <https://doi.org/10.1073/pnas.0604719103>

1217 Li, C., Deng, T., Wang, Y., Sun, F., Wolff, B., Jiangzuo, Q., Ma, J., Xing, L., Fu, J., Zhang, J., Wang, S.-Q.,
1218 2023. Longer mandible or nose? Co-evolution of feeding organs in early elephantiforms. *eLife*
1219 12. <https://doi.org/10.7554/eLife.90908.1>

1220 Liu, A.G.S.C., Seiffert, E.R., Simons, E.L., 2008. Stable isotope evidence for an amphibious phase in
1221 early proboscidean evolution. *Proceedings of the National Academy of Sciences* 105, 5786–
1222 5791. <https://doi.org/10.1073/pnas.0800884105>

1223 Luz, B., Kolodny, Y., Horowitz, M., 1984. Fractionation of oxygen isotopes between mammalian bone-
1224 phosphate and environmental drinking water. *Geochimica et Cosmochimica Acta* 48, 1689–
1225 1693.

1226 Ma, J., Wang, Y., Jin, C., Hu, Y., Bocherens, H., 2019. Ecological flexibility and differential survival of
1227 Pleistocene *Stegodon orientalis* and *Elephas maximus* in mainland southeast Asia revealed by
1228 stable isotope (C, O) analysis. *Quaternary Science Reviews* 212, 33–44.
1229 <https://doi.org/10.1016/j.quascirev.2019.03.021>

1230 Macfadden, B.J., Cerling, T.E., Harris, J.M., Prado, J., 1999. Ancient Latitudinal Gradients of C3/C4
1231 Grasses Interpreted from Stable Isotopes of New World Pleistocene Horse (*Equus*) Teeth.
1232 *Global Ecology and Biogeography* 8, 137–149.

1233 MacFadden, B.J., Morgan, G.S., Jones, D.S., Rincon, A.F., 2015. Gomphothere proboscidean
1234 (Gomphotherium) from the late Neogene of Panama. *Journal of Paleontology* 89, 360–365.
1235 <https://doi.org/10.1017/jpa.2014.31>

1236 Malferrari, D., Ferretti, A., Mascia, M.T., Savioli, M., Medici, L., 2019. How Much Can We Trust Major
1237 Element Quantification in Bioapatite Investigation? *ACS Omega* 4, 17814–17822.
1238 <https://doi.org/10.1021/acsomega.9b02426>

1239 Malhi, Y., Doughty, C.E., Galetti, M., Smith, F.A., Svenning, J.-C., Terborgh, J.W., 2016. Megafauna and
1240 ecosystem function from the Pleistocene to the Anthropocene. *Proceedings of the National
1241 Academy of Sciences* 113, 838–846. <https://doi.org/10.1073/pnas.1502540113>

1242 Martínez del Rio, C., Carleton, S.A., 2012. How fast and how faithful: the dynamics of isotopic
1243 incorporation into animal tissues. *Journal of Mammalogy* 93, 353–359.
1244 <https://doi.org/10.1644/11-MAMM-S-165.1>

1245 McMillan, R., Snoeck, C., de Winter, N.J., Claeys, P., Weis, D., 2019. Evaluating the impact of acetic
1246 acid chemical pre-treatment on ‘old’ and cremated bone with the ‘Perio-spot’ technique and
1247 ‘Perios-endos’ profiles. *Palaeogeography, Palaeoclimatology, Palaeoecology*.
1248 <https://doi.org/10.1016/j.palaeo.2019.05.019>

1249 Meckler, A.N., Sexton, P.F., Piasecki, A.M., Leutert, T.J., Marquardt, J., Ziegler, M., Agterhuis, T.,
1250 Lourens, L.J., Rae, J.W.B., Barnet, J., Tripathi, A., Bernasconi, S.M., 2022. Cenozoic evolution of
1251 deep ocean temperature from clumped isotope thermometry. *Science* 377, 86–90.
1252 <https://doi.org/10.1126/science.abk0604>

1253 Meinshausen, M., Nicholls, Z.R.J., Lewis, J., Gidden, M.J., Vogel, E., Freund, M., Beyerle, U., Gessner,
1254 C., Nauels, A., Bauer, N., Canadell, J.G., Daniel, J.S., John, A., Krummel, P.B., Luderer, G.,
1255 Meinshausen, N., Montzka, S.A., Rayner, P.J., Reimann, S., Smith, S.J., van den Berg, M.,
1256 Velders, G.J.M., Vollmer, M.K., Wang, R.H.J., 2020. The shared socio-economic pathway (SSP)
1257 greenhouse gas concentrations and their extensions to 2500. *Geoscientific Model
1258 Development* 13, 3571–3605. <https://doi.org/10.5194/gmd-13-3571-2020>

1259 Mellinger, M., 1979. Quantitative X-ray diffraction analysis of clay minerals: an evaluation.
1260 Saskatchewan Research Council.

1261 Metcalfe, J.Z., Longstaffe, F.J., 2012. Mammoth tooth enamel growth rates inferred from stable
1262 isotope analysis and histology. *Quaternary Research* 77, 424–432.
1263 <https://doi.org/10.1016/j.yqres.2012.02.002>

1264 Methner, K., Campani, M., Fiebig, J., Löffler, N., Kempf, O., Mulch, A., 2020. Middle Miocene long-
1265 term continental temperature change in and out of pace with marine climate records. *Sci Rep*
1266 10, 7989. <https://doi.org/10.1038/s41598-020-64743-5>

1267 Mothé, D., Ferretti, M.P., Avilla, L.S., 2016. The Dance of Tusks: Rediscovery of Lower Incisors in the
1268 Pan-American Proboscidean *Cuvieronius hyodon* Revises Incisor Evolution in
1269 *Elephantimorpha*. *PLoS One* 11, e0147009. <https://doi.org/10.1371/journal.pone.0147009>

1270 Nedoklan, S., Knezovic, Z., Knezovic, N., Sutlovic, D., 2021. NUTRITION AND MINERAL CONTENT IN
1271 HUMAN TEETH THROUGH THE CENTURIES. *Archives of Oral Biology* 124, 105075.
1272 <https://doi.org/10.1016/j.archoralbio.2021.105075>

1273 Oliveira, A., Rocha, F., Rodrigues, A., Jouanneau, J., Dias, A., Weber, O., Gomes, C., 2002. Clay minerals
1274 from the sedimentary cover from the Northwest Iberian shelf. *Progress in Oceanography*,
1275 Benthic processes and dynamics at the NW Iberian Margin: resultss of the OMEX II Program
1276 52, 233–247. [https://doi.org/10.1016/S0079-6611\(02\)00008-3](https://doi.org/10.1016/S0079-6611(02)00008-3)

1277 Pais, J., Cunha, P.P., Pereira, D., Legoinha, P., Dias, R., Moura, D., da Silveira, A.B., Kullberg, J.C.,
1278 González-Delgado, J.A., 2012. The Paleogene and Neogene of Western Iberia (Portugal): A
1279 Cenozoic Record in the European Atlantic Domain, in: Pais, J. (Ed.), *The Paleogene and
1280 Neogene of Western Iberia (Portugal): A Cenozoic Record in the European Atlantic Domain*,
1281 *SpringerBriefs in Earth Sciences*. Springer, Berlin, Heidelberg, pp. 1–138.
1282 https://doi.org/10.1007/978-3-642-22401-0_1

1283 Passey, B.H., Cerling, T.E., 2002. Tooth enamel mineralization in ungulates: implications for recovering
1284 a primary isotopic time-series. *Geochimica et Cosmochimica Acta* 66, 3225–3234.

1285 Patnaik, R., Singh, N.P., Paul, D., Sukumar, R., 2019. Dietary and habitat shifts in relation to climate of
1286 Neogene-Quaternary proboscideans and associated mammals of the Indian subcontinent.
1287 Quaternary Science Reviews 224, 105968. <https://doi.org/10.1016/j.quascirev.2019.105968>
1288 Pellegrini, M., Snoeck, C., 2016. Comparing bioapatite carbonate pre-treatments for isotopic
1289 measurements: Part 2—Impact on carbon and oxygen isotope compositions. Chemical
1290 Geology 420, 88–96.

1291 Quade, J., Cerling, T.E., Bowman, J.R., 1989. Development of Asian monsoon revealed by marked
1292 ecological shift during the latest Miocene in northern Pakistan. Nature 342, 163–166.
1293 <https://doi.org/10.1038/342163a0>

1294 Roberts, P., Stewart, M., Alagaili, A.N., Breeze, P., Candy, I., Drake, N., Groucutt, H.S., Scerri, E.M.L.,
1295 Lee-Thorp, J., Louys, J., Zalmout, I.S., Al-Mufarreah, Y.S.A., Zech, J., Alsharekh, A.M., al Omari,
1296 A., Boivin, N., Petraglia, M., 2018. Fossil herbivore stable isotopes reveal middle Pleistocene
1297 hominin palaeoenvironment in ‘Green Arabia.’ Nat Ecol Evol 2, 1871–1878.
1298 <https://doi.org/10.1038/s41559-018-0698-9>

1299 Sach, F., Dierenfeld, E.S., Langley-Evans, S.C., Watts, M.J., Yon, L., 2019. African savanna elephants
1300 (*Loxodonta africana*) as an example of a herbivore making movement choices based on
1301 nutritional needs. PeerJ 7, e6260. <https://doi.org/10.7717/peerj.6260>

1302 Saegusa, H., Nakaya, H., Kunimatsu, Y., Nakatsukasa, M., Tsujikawa, H., Sawada, Y., Saneyoshi, M.,
1303 Sakai, T., 2014. Earliest elephantid remains from the Late Miocene locality, Nakali, Kenya, in:
1304 Abstract Book of the VIth International Conference on Mammoths and Their Relatives.
1305 Scientific Annals of the School of Geology, Special. p. 175.

1306 Sakae, T., Mishima, H., Kozawa, Y., 1991. Proboscidea Fossil Teeth Suggest the Evolution of Enamel
1307 Crystals, in: Suga, S., Nakahara, H. (Eds.), Mechanisms and Phylogeny of Mineralization in
1308 Biological Systems. Springer Japan, Tokyo, pp. 477–481. https://doi.org/10.1007/978-4-431-68132-8_76

1309

1310 Sarna-Boś, K., Boguta, P., Skic, K., Wiącek, D., Maksymiuk, P., Sobieszcański, J., Chałas, R., 2022.
1311 Physicochemical Properties and Surface Characteristics of Ground Human Teeth. Molecules
1312 27, 5852. <https://doi.org/10.3390/molecules27185852>

1313 Schultz, L.G., 1964. Quantitative interpretation of mineralogical composition from X-ray and chemical
1314 data for the Pierre Shale. U.S. Geological Survey Professional Papers 391–C.

1315 Shaik, I., Dasari, B., Shaik, A., Doos, M., Kolli, H., Rana, D., Tiwari, R.V.C., 2021. Functional Role of
1316 Inorganic Trace Elements on Enamel and Dentin Formation: A Review. J Pharm Bioallied Sci
1317 13, S952–S956. https://doi.org/10.4103/jpbs.jpbs_392_21

1318 Sharma, V., Srinivasan, A., Nikolajeff, F., Kumar, S., 2021. Biomineralization process in hard tissues: The
1319 interaction complexity within protein and inorganic counterparts. Acta Biomaterialia,
1320 Biomineralization: From Cells to Biomaterials 120, 20–37.
1321 <https://doi.org/10.1016/j.actbio.2020.04.049>

1322 Shoshani, J., Tassy, P., 1996. The Proboscidea: evolution and palaeoecology of elephants and their
1323 relatives. Oxford University Press Oxford.

1324 Spencer, F., Verostick, K., Serna, A., Stantis, C., Bowen, G.J., 2024. Effects of particle size, storage
1325 conditions, and chemical pretreatments on carbon and oxygen isotopic measurements of
1326 modern tooth enamel. Science & Justice 64, 193–201.
1327 <https://doi.org/10.1016/j.scijus.2024.01.004>

1328 Staunton, S., Fairbridge, R.W., 2008. Duricrusts and Induration, in: Chesworth, W. (Ed.), Encyclopedia
1329 of Soil Science, Encyclopedia of Earth Sciences Series. Springer Netherlands, Dordrecht, pp.
1330 192–198. https://doi.org/10.1007/978-1-4020-3995-9_168

1331 Steinhorsdottir, M., Coxall, H.K., Boer, A.M. de, Huber, M., Barbolini, N., Bradshaw, C.D., Burls, N.J.,
1332 Feakins, S.J., Gasson, E., Henderiks, J., Holbourn, A., Kiel, S., Kohn, M.J., Knorr, G., Kürschner,
1333 W.M., Lear, C.H., Liebrand, D., Lunt, D.J., Mörs, T., Pearson, P.N., Pound, M.J., Stoll, H.,
1334 Strömberg, C. a. E., 2020. The Miocene: the Future of the Past. Paleoclimatology and
1335 Paleoclimatology n/a, e2020PA004037. <https://doi.org/10.1029/2020PA004037>

1336 Suba, R.B., Beveridge, N.G., de Jongh, H.H., de Snoo, G.R., 2016. Bornean elephant food preference
1337 based on Nuclear Magnetic Resonance (NMR) metabolic profiling techniques.

1338 Super, J.R., Thomas, E., Pagani, M., Huber, M., O'Brien, C., Hull, P.M., 2018. North Atlantic
1339 temperature and pCO₂ coupling in the early-middle Miocene. *Geology* 46, 519–522.
1340 <https://doi.org/10.1130/G40228.1>

1341 Tejada-Lara, J.V., MacFadden, B.J., Bermudez, L., Rojas, G., Salas-Gismondi, R., Flynn, J.J., 2018. Body
1342 mass predicts isotope enrichment in herbivorous mammals. *Proc Biol Sci* 285, 20181020.
1343 <https://doi.org/10.1098/rspb.2018.1020>

1344 Thorez, J., 1976. Practical identification of clay minerals: A handbook for teachers and students in clay
1345 mineralogy. Dison, Belgique.

1346 Tipple, B.J., Meyers, S.R., Pagani, M., 2010. Carbon isotope ratio of Cenozoic CO₂: A comparative
1347 evaluation of available geochemical proxies. *Paleoceanography* 25.
1348 <https://doi.org/10.1029/2009PA001851>

1349 Tütken, T., Furrer, H., Walter Vennemann, T., 2007. Stable isotope compositions of mammoth teeth
1350 from Niederweningen, Switzerland: Implications for the Late Pleistocene climate,
1351 environment, and diet. *Quaternary International, From the Swiss Alps to the Crimean
1352 Mountains - Alpine Quaternary stratigraphy in a European context* 164–165, 139–150.
1353 <https://doi.org/10.1016/j.quaint.2006.09.004>

1354 Ullmann, C.V., Korte, C., 2015. Diagenetic alteration in low-Mg calcite from macrofossils: a review.
1355 *Geological Quarterly* 59, 3–20, doi: 10.7306/gq.1217. <https://doi.org/10.7306/gq.1217>

1356 Uno, K.T., Fisher, D.C., Wittemyer, G., Douglas-Hamilton, I., Carpenter, N., Omondi, P., Cerling, T.E.,
1357 2020. Forward and inverse methods for extracting climate and diet information from stable
1358 isotope profiles in proboscidean molars. *Quaternary International, High resolution analyses
1359 of large mammals dental remains: broadening horizons* 557, 92–109.
1360 <https://doi.org/10.1016/j.quaint.2020.06.030>

1361 van der Merwe, N.J., Medina, E., 1991. The canopy effect, carbon isotope ratios and foodwebs in
1362 amazonia. *Journal of Archaeological Science* 18, 249–259. [https://doi.org/10.1016/0305-
1363 4403\(91\)90064-V](https://doi.org/10.1016/0305-4403(91)90064-V)

1364 Vansteenberge, S., de Winter, N.J., Sinnesael, M., Xueqin, Z., Verheyden, S., Claeys, P., 2020. Benchtop
1365 μ XRF as a tool for speleothem trace elemental analysis: Validation, limitations and application
1366 on an Eemian to early Weichselian (125–97 ka) stalagmite from Belgium. *Palaeogeography,
1367 Palaeoclimatology, Palaeoecology* 538, 109460.
1368 <https://doi.org/10.1016/j.palaeo.2019.109460>

1369 Vogel, J.C., 1980. Fractionation of the Carbon Isotopes During Photosynthesis. Springer Science &
1370 Business Media.

1371 Wang, J., Zhou, X., Wang, S., Xu, H., Behling, H., Ye, J., Zheng, Y., Liu, J., Wu, Y., Zhao, K., Zhang, R., Li,
1372 X., 2023. C₄ expansion of Central Asia in the middle Miocene linked to the strengthening
1373 Indian monsoon. *Global and Planetary Change* 224, 104096.
1374 <https://doi.org/10.1016/j.gloplacha.2023.104096>

1375 Wang, S.-Q., Li, Y., Duangkrayom, J., Yang, X.-W., He, W., Chen, S.-Q., 2017. A new species of
1376 Gomphotherium (Proboscidea, Mammalia) from China and the evolution of Gomphotherium
1377 in Eurasia. *Journal of Vertebrate Paleontology* 37, e1318284.
1378 <https://doi.org/10.1080/02724634.2017.1318284>

1379 Wang, W., Liao, W., Li, D., Tian, F., 2014. Early Pleistocene large-mammal fauna associated with
1380 Gigantopithecus at Mohui Cave, Bubing Basin, South China. *Quaternary International,
1381 Multidisciplinary Perspectives on the Gigantopithecus Fauna and Quaternary Biostratigraphy
1382 in East Asia* 354, 122–130. <https://doi.org/10.1016/j.quaint.2014.06.036>

1383 Water Isotopes Database [WWW Document], 2023. URL
1384 https://wateriso.utah.edu/waterisotopes/pages/spatial_db/SPATIAL_DB.html (accessed
1385 10.25.23).

1386 Westerhold, T., Marwan, N., Drury, A.J., Liebrand, D., Agnini, C., Anagnostou, E., Barnet, J.S., Bohaty,
 1387 S.M., De Vleeschouwer, D., Florindo, F., 2020. An astronomically dated record of Earth's
 1388 climate and its predictability over the last 66 million years. *Science* 369, 1383–1387.
 1389 What Did Lupe Eat? - Mammoth Discovery [WWW Document], n.d. URL
 1390 <https://www.cdm.org/mammothdiscovery/lupeeat.html> (accessed 1.10.24).
 1391 Wheelock, N., 1980. Environmental Sodium as a Factor in the Behavior and Distribution of African
 1392 Elephants. *Elephant* 1. <https://doi.org/10.22237/elephant/1521731760>
 1393 Wood, R., Fleury, A.B.C., Fallon, S., Nguyen, T.M.H., Nguyen, A.T., 2021. DO WEAK OR STRONG ACIDS
 1394 REMOVE CARBONATE CONTAMINATION FROM ANCIENT TOOTH ENAMEL MORE
 1395 EFFECTIVELY? THE EFFECT OF ACID PRETREATMENT ON RADIOCARBON AND $\delta^{13}C$ ANALYSES.
 1396 *Radiocarbon* 63, 935–952. <https://doi.org/10.1017/RDC.2021.32>
 1397 Wooller, M.J., Bataille, C., Druckenmiller, P., Erickson, G.M., Groves, P., Haubenstein, N., Howe, T.,
 1398 Irrgeher, J., Mann, D., Moon, K., Potter, B.A., Prohaska, T., Rasic, J., Reuther, J., Shapiro, B.,
 1399 Spaleta, K.J., Willis, A.D., 2021. Lifetime mobility of an Arctic woolly mammoth. *Science* 373,
 1400 806–808. <https://doi.org/10.1126/science.abg1134>
 1401 Wu, Y., Deng, T., Hu, Y., Ma, J., Zhou, X., Mao, L., Zhang, H., Ye, J., Wang, S.-Q., 2018. A grazing
 1402 Gomphotherium in Middle Miocene Central Asia, 10 million years prior to the origin of the
 1403 Elephantidae. *Sci Rep* 8, 7640. <https://doi.org/10.1038/s41598-018-25909-4>
 1404 Zachos, J., Pagani, M., Sloan, L., Thomas, E., Billups, K., 2001. Trends, rhythms, and aberrations in
 1405 global climate 65 Ma to present. *Science* 292, 686–693.
 1406 Zachos, J.C., Dickens, G.R., Zeebe, R.E., 2008. An early Cenozoic perspective on greenhouse warming
 1407 and carbon-cycle dynamics. *Nature* 451, 279.
 1408